Targeted ablation and regeneration of enteric nervous system neurons in zebrafish

Mujahid Ali Shah[1], Katherine K. Moran[1], Helen Rueckert[1,2], Abigail V. Sharrock[3], David F. Ackerley[3], Jeff S. Mumm[4], Julia Ganz[1] *

[1]Department of Integrative Biology, Michigan State University, East Lansing, MI, USA, [2]Department of Cell Biology, Developmental and Stem Cell Biology Program, Duke University School of Medicine, Durham, NC, USA, [3]School of Biological Sciences, Victoria University of Wellington, Wellington, New Zealand, [4] Department of Ophthalmology, Wilmer Eye Institute, Johns Hopkins University, Baltimore, MD, USA.

***Correspondence**, ganz@msu.edu

Abstract

The enteric nervous system (ENS) is the intrinsic nervous system of the gut and regulates essential gut functions, including motility, digestion, and immune response, ensuring gut homeostasis. ENS dysfunction or loss is associated with gastrointestinal disorders such as Hirschsprung disease (HSCR). Currently, surgery is the only treatment for HSCR, but it often has lifelong, severe complications. Restoring missing ENS neurons by stimulating endogenous neuronal regeneration presents a promising therapeutic approach for ENS disease. To study the cellular-molecular mechanisms of neuronal regeneration we first need to identify an animal model system with robust ENS regeneration. For this, we developed a chemical-genetic ablation model in zebrafish using the Gal4/UAS NTR 2.0 system for targeted ENS neuron ablation. Spatially and temporally controlled neuronal death was confirmed by morphological changes, complete neuronal loss, and TUNEL assays. Quantification of regenerated neurons demonstrated complete restoration of ENS neuron numbers to control levels by 9 days post treatment with recovery of gut motility. Among the regenerated neurons, nitrergic, cholinergic and vipergic subtypes showed full recovery, whereas serotonergic neurons only displayed partial recovery, indicating subtype-specific differences in the regenerative capacity and/or timing. Our study establishes a robust platform for dissecting the cellular-molecular mechanisms of ENS regeneration to develop potential treatment approaches for ENS-related diseases.

Keywords: Enteric neurons, chemical-genetic ablation, functional recovery, gut motility, ENS diseases

Introduction

The enteric nervous system (ENS), the largest subdivision of the peripheral nervous system, consists of an intricate network of neurons and glial cells derived from neural crest progenitors that migrate into the developing gastrointestinal tract (Ganz, 2018; Hao & Young, 2009; Taylor et al., 2016). This complex network plays a pivotal role in regulating essential gastrointestinal functions such as gut motility, nutrient absorption, epithelial secretion, and blood flow (Kuil et al., 2021; Kunze & Furness, 1999; Niesler et al., 2021). Dysfunction or loss of the ENS has been linked to various gastrointestinal disorders such as Hirschsprung disease (HSCR), Achalasia, and autism spectrum disorder (Niesler et al., 2021). HSCR, which is characterized by aganglionosis in the distal gut, is one of the most common congenital anomalies of the ENS, leading to severe intestinal obstruction in neonates, with an estimated incidence of 1 in 5,000 live births (Butler Tjaden & Trainor, 2013). To date, ENS disorders can only be treated symptomatically or by surgical removal of the area with ENS neuron deficits. For example, the current standard treatment for HSCR is surgical resection of the aganglionic gut segment. However, patient outcomes vary widely, and most continue to experience lifelong gastrointestinal defects, highlighting the need for alternative treatments. One of the therapeutic approaches for HSCR is the stimulation of resident stem cells to regenerate missing ENS cells with promising results but varying efficacy depending on the age and the specific gut region (Burns et al., 2016; Joseph et al., 2011; Soret et al., 2020). The successful translation of these approaches requires a comprehensive understanding of the cellular and molecular mechanisms that underlie effective ENS regeneration. Elucidating these mechanisms necessitates the development of a reliable animal model that exhibits robust and reproducible regeneration of ENS neurons following injury.

So far, only few studies - mostly in mammalian models - have investigated ENS regeneration using chemical, mechanical, or chemical-genetic injury. Although these approaches have provided valuable insights, mammalian models show limited and incomplete neuronal regeneration in the ENS (Rueckert & Ganz, 2022; Stavely et al., 2024). In contrast, the zebrafish (*Danio rerio*), a non-mammalian animal model system is a robust model for studying organ regeneration including various parts of the nervous system such as the brain (Kizil et al., 2012) retina (Hanovice et al., 2019), ENS (El-Nachef & Bronner, 2020; Ohno et al., 2021), but also other organs, such as kidney (Elmonem et al., 2018), heart (Cao & Poss, 2018), and fin (Romero et al., 2018). Zebrafish also offer numerous experimental advantages, including rapid development, large numbers of offspring, optical transparency that enables live imaging, and a high degree of genetic homology with humans (Howe et al., 2013). Despite these experimental advantages (Kuil et al., 2021; Ganz, 2018), so far, only two studies have studied ENS regeneration in zebrafish using a laser ablation approach (El-

Nachef & Bronner, 2020; Ohno et al., 2021). Those studies provide first evidence that the ENS can regenerate in zebrafish following laser ablation. Ohno et al., show that neural crest-derived cells migrate into the ablated region, proliferate, and give rise to new neurons, partially restoring ENS neuron numbers. However, several important issues to demonstrate that the ENS fully regenerates in zebrafish remain: First, the number of regenerated neurons did not reach control levels in the studied time frame. Second, it remains to be shown which neuronal subtypes are ablated and are able to regenerate. Third, it remains unclear whether the regenerated neurons functionally integrated into existing ENS circuits to re-establish normal gut function. In addition, laser ablation has several technical limitations, including collateral damage to surrounding tissues, labor-intensive protocols, and restricted ablation of just a few cells within a small gut region, hindering downstream analysis for functional recovery assessment (Ohno et al., 2021).

To overcome these challenges, we leveraged an established approach for spatiotemporally controlled cell ablation: the chemical-genetic bacterial nitroreductase (NTR) system. This method utilizes the NTR enzyme, which converts prodrugs, e.g., Metronidazole (MTZ), into cytotoxic agents, thereby selectively killing cells that express NTR (Bridgewater et al., 1995). In zebrafish, this chemical-genetic method has been successfully applied in regenerative studies by ablating specific cell populations in heart, pancreas, liver, retina, and rod photoreceptor cell (Ariga et al., 2010; Curado et al., 2007, Sharrock et al., 2022; White et al., 2017). However, this method has not yet been tested for the ablation of ENS neurons.

In this study, we took advantage of the precise spatial-temporal control of the *Gal4/UAS* system (Asakawa et al., 2008; Zhang et al., 2019) for the chemical-genetic ablation of ENS neurons in postembryonic zebrafish larvae (**Figure 1**). We additionally employed the most advanced iteration of the nitroreductase technology, NTR 2.0, which provides effective ablation of target cells at ~100-fold lower concentrations of MTZ than the original NTR system (Sharrock et al., 2022). Using this approach, we establish a robust experimental paradigm of ENS neuron regeneration by ablating only NTR-expressing neurons through MTZ treatment. Morphological and TUNEL analysis confirmed that the ablated cells underwent cell death. By 9 day post treatment (dpt), neuronal recovery was complete, with full recovery of most neuronal subtypes, including nitrergic, cholinergic and vipergic neurons. Our results demonstrate for the first time functional recovery of ENS neuron numbers including restoration of gut motility. These findings pave the way for understanding the cellular and molecular mechanisms of ENS regeneration, which will provide the first step for developing new therapeutic approaches for gastrointestinal disorders associated with ENS dysfunction in the future.

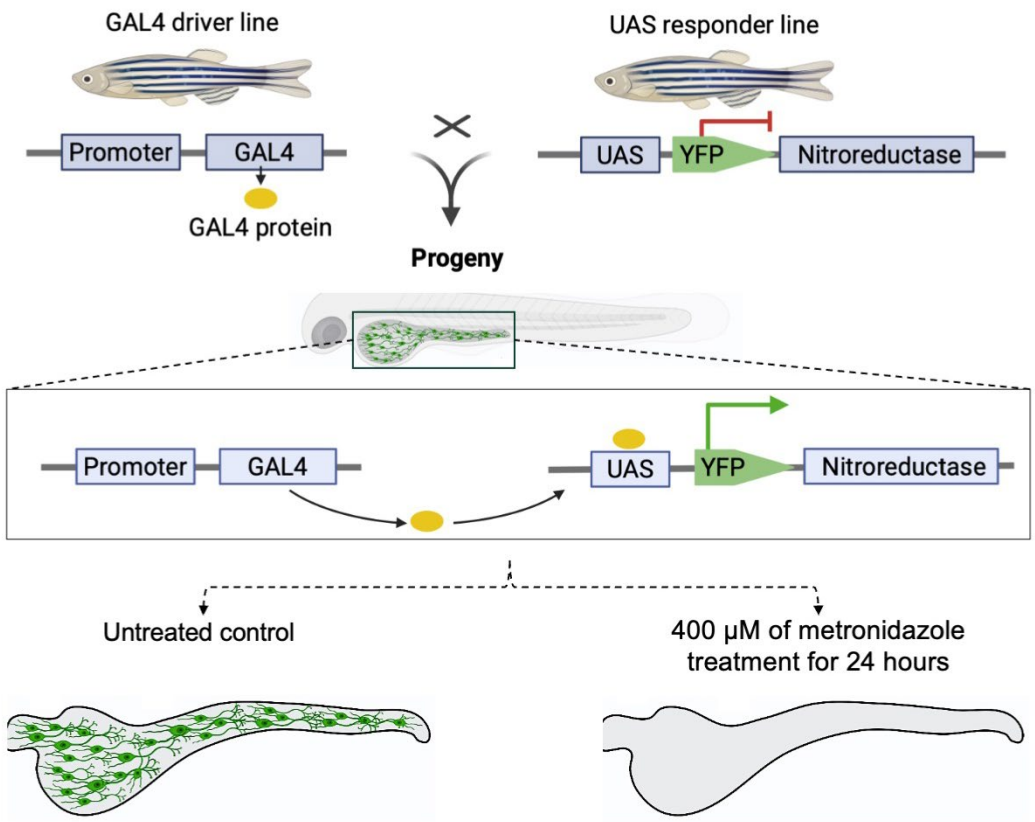

Figure 1 Experimental setup for ENS neuron ablation in zebrafish

A carrier of the Gal4 driver line, *Tg*(*217B:Gal4)*, which drives expression in ENS neurons was crossed with a carrier of the responder/effector line *Tg(UAS:YFP-NTR 2.0)*, where the Gal4 protein binds to Upstream Activating Sequence (*UAS*) element, initiating expression of both *yellow fluorescence protein* (YFP, reporter protein) and *nitroreductase* (NTR 2.0). Left side: Schematic representation of the untreated control intestine, where enteric neurons co-expressing the *Gal4* and *UAS* transgenes also express both YFP and NTR 2.0 in ENS neurons (green). Right side: Schematic representation of intestine following treatment with 400 µM metronidazole (MTZ). The prodrug MTZ is enzymatically converted by NTR 2.0 into a cytotoxic compound, leading to the selective ablation of YFP-NTR 2.0-expressing enteric neurons.

Material and methods

Animals

All experiments were carried out in accordance with animal welfare laws, guidelines, and policies and were approved by the Michigan State University Institutional Animal Care and Use

107 Committee. Zebrafish lines were maintained in a laboratory breeding colony according to
108 established protocols (Westerfield, 2000). Adult zebrafish were bred naturally in system water,
109 and fertilized eggs were collected and transferred to 100 mm petri dishes containing embryo
110 medium. Embryos were allowed to develop at 28.5°C and staged by days post fertilization (dpf)
111 as described earlier (Kimmel, 1995; Webb et al., 2009). The zebrafish lines utilized in this study
112 are listed in **Table 1**. Double transgenic larvae were established to co-express YFP and NTR
113 2.0 in the nervous system. For this, the *Tg(5xUAS:GAP-TagYFP-2A-NTR2.0)jh513Tg*
114 reporter/effector line was maintained together with the *Et(2xNRSE-cfos KALT4)gmc617;*
115 *Tg(5xUAS:GAP-ECFP,he1.1:GAP-ECFP)gmc1913* transgenic fish line. The
116 *Et(2xNRSE:cfos:KalTA4)gmc617* line expresses KalTA4, a zebrafish-optimized Gal4/VP16
117 fusion protein with neuronal specificity (Xie et al., 2012; Sharrock et al., 2022). We confirmed
118 that the *Tg(SAGFF(LF)217B)* drives reporter expression in ENS neurons (described in the
119 results section), as an incross of *Tg(5xUAS:GAP-TagYFP-2A-NTR2.0)*; *Et(2xNRSE-cfos*
120 *KALT4)gmc617; Tg(5xUAS:GAP-ECFP,he1.1:GAP-ECFP)gmc1913* did not show YFP
121 expression in ENS neurons. The *Tg(5xUAS:GAP-ECFP,he1.1:GAP-ECFP)gmc1913* line
122 expresses cyan fluorescent protein (CFP), our analysis was focused on YFP expression driven
123 by the Gal4/UAS system. Genotyping of Gal4 driver lines was performed with the following
124 primers for Gal4 (GAL4F: 5'-CGCTACTCTCCCAAAACCAAAAGG-3'; GAL4R: 5'-
125 TCTCTTCCGATGATGATGTCGCAC -3' using the PCR protocol: 95° x 3 min - [95° x 30s - 60° x
126 30s - 72° x 30s] x 35 - 72° x 5' 12° ∞.

127 **Table 1: Transgenic lines used in this study**

Full name	Abbreviation	Source
Tg(SAGFF(LF)217B)	*217B:Gal4*	Asakawa et al., 2008
Tg(SAGFF(LF)234A)	*234A:Gal4*	Asakawa et al., 2008
Tg(gSAIzGFFM495A)	*495A:Gal4*	Kawakami et al., 2010
Tg(5xUAS:EGFP)nkuasgfp	*UAS:GFP*	Asakawa et al., 2008
Tg(UAS-E1b:NfsB-mCherry)c264	*UAS:NTR-mCherry*	Davison et al., 2007
Tg(5xUAS:GAP-TagYFP-2A-NTR2.0)jh513Tg; Et(2xNRSE-cfos KALT4)gmc617; Tg(5xUAS:GAP-ECFP, he1.1:GAP-ECFP)gmc1913	*UAS:YFP-NTR 2.0**	Sharrock et al., 2022; Xie et al., 2012

128 *The *Tg(5xUAS:GAP-TagYFP-2A-NTR2.0)jh513Tg* fish were maintained together with the *Et(2xNRSE-cfos*
129 *KALT4)gmc617; Tg(5xUAS:GAP-ECFP,he1.1:GAP-ECFP)gmc1913* lines.
130
131
132

133 **Chemical-genetic ablation using Metronidazole**

134 The *217B:Gal4* driver line was crossed with the *UAS:YFP-NTR 2.0* responder line. Offspring
135 from this cross were sorted based on YFP+ cells in the gut into YFP+ and YFP− groups at 5 dpf
136 using a Zeiss Axio ZoomV16 fluorescent stereo microscope. The sorted larvae were then
137 treated at 5 dpf or for the later time point transferred to the nursery until the day of the assay.
138 Prior to MTZ treatment, larvae - except for the 5 dpf groups - were starved for 24 hours to clear
139 the gut of autofluorescent matter. Approximately 50 larvae were transferred to a petri dish (100
140 mm × 15 mm) containing 40 mL of 400 μM MTZ (M1547 Sigma Aldrich) (Sharrock et al., 2022)
141 in zebrafish system water (diluted from a 5mM stock solution). The following experimental
142 groups were used: 1) YFP+ MTZ (YFP+ larvae treated with MTZ; 2) YFP+ control (YFP+ larvae,
143 not treated with MTZ); and 3) YFP- MTZ (YFP- larvae, treated with MTZ). Larvae were
144 incubated in the dark for 24 hours to ensure maximal drug exposure as MTZ is light sensitive.
145 After 24 hours, the effects of MTZ treatment on YFP+ cell ablation were assessed using a Zeiss
146 Axio Zoom.V16 fluorescent stereo microscope. After confirmation of cell loss, the MTZ solution
147 was discarded and larvae were returned to the nursery, placed in 2.8-liter tanks (~40 larvae per
148 tank), and raised until the indicated experimental time point.

149

150 **ENS neuron regeneration analysis**

151 The regeneration of MTZ-treated YFP+ cells in the gut was assessed at 12 dpf (0 dpt, before
152 ablation) and subsequently at three-day intervals from 13 dpf (1 dpt) to 27 dpf (15 dpt) and
153 compared to YFP+ untreated controls. At each regeneration time point, both control and treated
154 larvae were checked briefly using a Zeiss Axio Zoom.V16 fluorescent stereo microscope, then
155 fixed and immunoassayed (as described below) by confocal microscopy imaging for data
156 acquisition.

157

158 **Sample fixation**

159 To ensure optimal imaging conditions, larvae were fasted for 24 hours prior to sampling at the
160 required stages to allow for gut clearance of autofluorescent matter. Then, larvae were
161 euthanized with an overdose of Tricaine Methanesulfonate (MS-222). **For immunolabeling**,
162 euthanized samples were fixed in 4% paraformaldehyde (PFA) prepared in 1x sweet buffer (8%
163 sucrose, 0.2 M $CaCl_2$, 0.2 M PO_4 buffer, pH 7.3) for 2 hours at room temperature. Then, they
164 were washed subsequently 2 times in 0.5% Phosphate buffer saline-Triton™ X-100 (PBSTX) for
165 15 mins at room temperature, and stored in PBSTX at 4°C**. For TUNEL assay**, euthanized
166 samples were fixed overnight in 10% Natural buffer saline (NBF) at 4°C, then washed three

167 times in PBS for 5 minutes at room temperature and stored in PBS at 4°C. **For Hybridization**
168 **Chain Reaction (HCR)**, euthanized larvae were rinsed thoroughly in RNAase free water, and
169 fixed in RNAase free 4% PFA in PBS at 4°C for ~16 hours, washed three times in PBS for 5
170 minutes at room temperature, dehydrated in a graded methanol series (50, 70, 90, 95 and 100
171 % methanol in nuclease free water), and stored in 100% methanol at −20°C for a minimum of
172 16 hours or up to six months (Ibarra-García-Padilla et al., 2021).
173
174 **TUNEL assay**
175 TUNEL assays were performed using the Click-iT™ Plus TUNEL Assay Kits (C10618, Thermo
176 Fisher Scientific) for In Situ Apoptosis Detection. For this, PBS was removed from fixed samples
177 and permeabilization was carried out using Proteinase K (20 µg/mL) for 50 minutes at room
178 temperature, followed by three PBS washes and a deionized water rinse. Then samples were
179 re-fixed in 10% NBF in PBS for 5 minutes at 37°C, followed by three additional PBS washes and
180 another deionized water rinse. To detect DNA strand breaks (i.e., for the positive control), the
181 larvae were incubated in 1 unit of DNase I (Cat. No. 18068-015) diluted into 1X DNase I
182 Reaction Buffer for 30 minutes at room temperature (**Figure S1)**. After that, larvae were
183 preincubated in 150 µL of Terminal deoxynucleotidyl transferase (TdT) buffer for 10 minutes at
184 37°C, incubated in the 100 µL TdT reaction mixture {94 µL TdT Reaction Buffer, 2 µL 5-ethynyl-
185 2'-deoxyuridine-5'-triphosphate (EdUTP), and 4 µL TdT enzyme} for 30 minutes at 37°C, rinsed
186 in deionized water, washed twice in 3 % bovine serum albumin (BSA) in 0.1% PBS-Triton™ X-
187 100 for 5 minutes each, and one time in PBS. Then the larvae were incubated with the reaction
188 cocktail (90 µL TUNEL Supermix and 10 µL 10X Click-iT Plus TUNEL Reaction Buffer Additive)
189 for 30 minutes at 37°C in the dark, followed by two 3% BSA in PBS washes and two final PBS
190 washes. TUNEL staining was assessed using a Zeiss Axio Zoom.V16 fluorescence
191 stereomicroscope. Immunostaining was subsequently performed under dark conditions, as
192 described below, and larvae were stored in PBS until imaging.
193
194 **Immunostaining**
195 Whole-mount immunostaining was performed as previously described (Bandla et al., 2022;
196 Uyttebroek et al., 2010). The following primary antibodies: 5-HT (1:5,000, catalog number
197 20080), HuC/D (1:1,000, catalog number A-21271), mouse GFP (1:300, catalog number
198 A11120), rabbit GFP (1:1,000, catalog number A11122), and nNOS (1:1,000, catalog number
199 GTX133407) were utilized to perform immunostaining. The primary antibodies were detected
200 using Alexa Fluor 488 and/or 568 secondary antibodies, followed by washes with 0.3% PBSTX.

201 The staining was assessed using Zeiss Axio Zoom.V16 fluorescent stereo microscope and
202 samples were stored in 0.3% PBSTX at 4°C until imaging.
203
204 **Hybridization Chain Reaction**
205 The (HCR) kit, probes, *vip* (Accession number: NM_001114553.3) and *slc18a3a* (Accession
206 number: NM_001077550.1), and hairpins were from Molecular Instruments, Inc.
207 (https://www.molecularinstruments.com) and the HCR protocol was performed as previously
208 described (Ibarra-García-Padilla et al., 2021) with minor modifications. The HCR protocol was
209 followed by immunostaining. The fixed samples stored in 100% methanol were rehydrated in
210 graded methanol series, permeabilized with pre-chilled acetone at −20°C for 25 min, treated
211 with 20 µg of Proteinase K for 1 h at room temperature, refixed in 4% PFA in PBS for 20 min,
212 and washed with PBS-Tween before hybridization. For HCR hybridization, samples were pre-
213 hybridized at 37°C, incubated with a probe mixture (4 µL of each 1 µM probe set stock) for 12–
214 16 hours, washed to remove excess probes, and amplified for 12–16 hours, followed by
215 sequential washes (Ibarra-García-Padilla et al., 2021). For antibody staining, samples were
216 blocked in 5% goat serum, incubated with primary anti-mouse GFP (1:300, catalog number
217 A11120) antibodies overnight at 4°C, washed extensively, and incubated with secondary
218 antibodies overnight (Ibarra-García-Padilla et al., 2021). Throughout the protocol, samples were
219 protected from light to prevent photobleaching, ensuring optimal visualization of hybridization
220 and staining results. Afterward, stained samples were stored in PBST at 4°C until imaging.
221
222 **Imaging, data acquisition, and quantification**
223 For analysis of colocalization and quantification, intestines were dissected with forceps and
224 mounted on glass slides in 0.3% PBSTX and covered with a coverslip. For the analysis of Gal4-
225 based reporter co-expression with the pan-neuronal marker HuC/D, mounted intestines were
226 imaged on a Zeiss Axio Imager microscope operated through the ZEN software to determine
227 colocalization. Confocal z-stacks images were captured using the 3i spinning disk confocal
228 microscope with a 10, 20, or 60× objectives, operated through Slidebook6 software (Version
229 6.0.13). For cell quantification, z-stacks were generated from confocal stacks in Slidebook6,
230 which were used for manual cell counts and colocalization analysis. For analysis within gut
231 regions, the images of the intestine were divided into three sections - anterior, middle, and
232 posterior - as previously described (Jianlong Li et al., 2024; Wallace et al., 2005). Cell counts
233 were normalized to 200 µm to account for varying lengths of each of gut regions between larvae
234 and to 1000 µm for the whole gut.

235 **Analysis of neuron morphology**

236 To analyze morphological changes in neurons after MTZ exposure, control and MTZ-treated
237 larvae were euthanized at the timepoint indicated, their intestines were dissected, mounted on
238 glass slide in PBS and imaged on the 3i spinning disk confocal microscope with a 60× objective,
239 operated through Slidebook6 software (Version 6.0.13).

240

241 **Gut anterograde movements analysis**

242 Larvae from control and treated groups were fasted 24 hours prior to analysis, anesthetized with
243 MS-222, and embedded in 0.8% low-melting-point agarose. Videos of the gut region from
244 midgut to posterior were recorded on the Zeiss Axio Zoom.V16 fluorescent stereo microscope
245 with ZEN Imaging Software (ZEN 2.3 blue edition). All time lapse videos were recorded using
246 the same conditions, including exposure time (206s), frame rate (100 frames / 206 sec), and
247 pixels (2752 x 2208). The total number of anterograde, peristaltic wave movements was
248 analyzed from the recorded videos. The Peristaltic Wave Interval (PWI) time was calculated as:
249 PWI = T/N where PWI represents the average time interval (in seconds) between two
250 consecutive anterograde peristaltic movements. The total duration of each video (T, in seconds)
251 and the total number of peristaltic movements observed (N) were recorded.

252

253 **Statistical Analysis**

254 For multiple comparisons, one-way and two-way ANOVA were applied to normally distributed
255 data, while the non-parametric Kruskal–Wallis test was used when the data violated the
256 assumption of normality. For pairwise comparisons, unpaired t-tests were used for normally
257 distributed data, and the Mann–Whitney test was used for non-normally distributed data. To
258 evaluate temporal changes across multiple time points in regeneration studies, multiple
259 unpaired t-tests were performed between MTZ-treated and control larvae. For fractional analysis
260 of neuronal colocalization patterns, descriptive statistics were applied. All statistical analyses
261 were performed using GraphPad Prism 9.1 (GraphPad Software, San Diego, CA, USA). A
262 significance threshold of $p < 0.05$ was used to determine statistically significant differences.

263

264

265

266

267

268

Results

Identification of Gal4 driver line for specific ablation of ENS neurons

To identify a Gal4 driver line for maximizing the breadth and selectivity of ENS neuron ablations, we crossed three Gal4 gene-trap driver lines (*495A:Gal4; 234A:Gal4; 217B:Gal4*) with a *UAS* reporter line to analyze the extent and specificity of reporter gene expression in the ENS and surrounding tissues. To determine if reporter gene expression is primarily restricted to ENS neurons, thereby minimizing off-target ablation, we investigated reporter gene co-expression with the pan-neuronal marker HuC/D in the ENS at 5 dpf (*495A:Gal4xUAS:GFP*, *234A:Gal4xUAS:NTR:DsRed*) and at 5, 6 and 7 dpf (*217B:Gal4xUAS:GFP*, **Figure 2**). Our analysis revealed notable differences in the co-expression profiles among the driver lines. Intestines of the *234A:Gal4* and *217B:Gal4* driver lines exhibited higher number of neurons co-expressing HuC/D+ and Reporter with only a small population of HuC/D-/Reporter+ and HuC/D+/Reporter- cells (**Figure 2A-B**). In contrast, intestines of the *495A:Gal4* line displayed only about half HuC/D+/Reporter+ cells with many reporter+ cells being HuC/D- and HuC/D+/Reporter- cells (**Figure 2A**). Comparatively, both the *234A:Gal4* and *217B:Gal4* lines had sufficient Reporter+ cells in the gut. However, *234A:Gal4* drives extensive reporter gene expression outside the ENS and in ENS progenitor cells (Heanue et al., 2016), which would lead to ablation of additional, non-targeted cells. Therefore, we chose the *217B:Gal4* line to maximize the extent and specificity of ENS neuron ablation (**Figure 2B**).

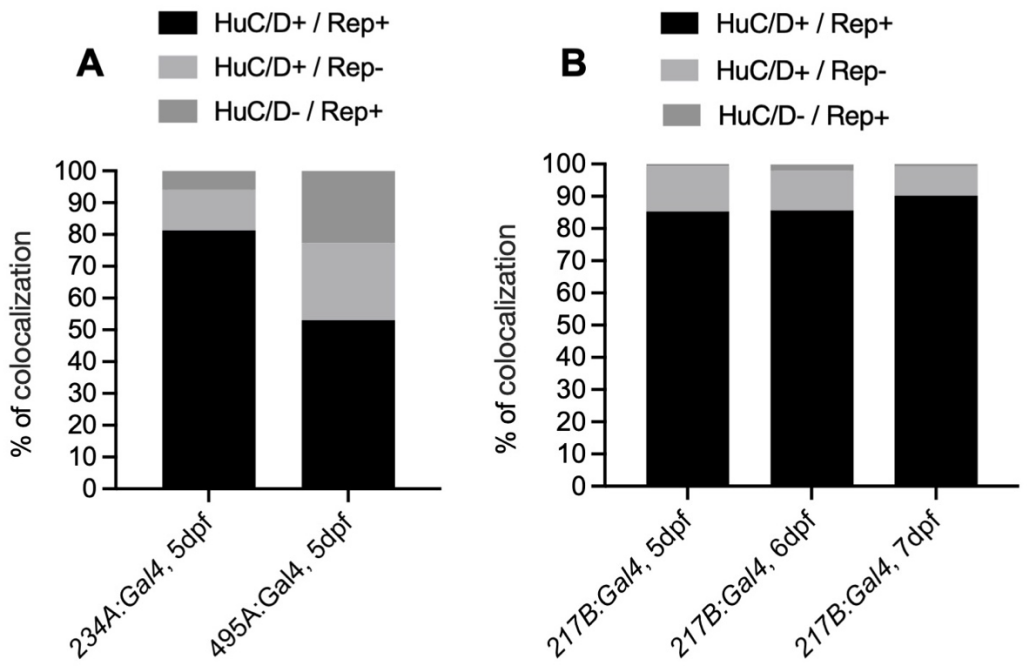

Figure 2. Identification of Gal4 driver line for specific ENS neuron ablation. (A-B) The bar graphs show colocalization percentage of the pan-neuronal marker HuC/D with Reporter (Rep) expression within the gut for Gal4 driver. **(A)** For the *234A:Gal4* line, most Rep+ cells are HuC/D+ at 5 dpf (81.3% HuC/D+/Rep+). The remaining cells consist of 12.7% HuC/D+/ Rep- and 6.0% HuC/D-/Rep+ (n = 12 larvae, 2 experiments). For the *495A:Gal* line, only 55% cells are HuC/D+/Rep+ at 5 dpf, the remaining cells are 23.5% HuC/D+/ Rep- and 21.2% HuC/D-/Rep+ (n = 12 larvae, 2 experiments). **(B)** For the *217B:Gal4* line, there is a high degree of overlap between Rep and HuC/D expression {(85.3% (5dpf), 85.7% (6dpf), and 90.2% (7dpf)}. The remaining cells consist of HuC/D+/ Rep- {14% (5dpf) 12.3% (6dpf) and 9.0% (7 dpf)} and HuC/D-/Rep+ {0.7% (5dpf), 2.0% (6dpf), and 0.8% (7 dpf)}, n = 13 (5dpf), 15 (6dpf), and 14 (7dpf) larvae, 2 experiments per time point. dpf = days post fertilization.

Establishing a robust chemical-genetic ablation assay for ENS neuron

To establish a robust ENS neuron ablation assay, we used offspring from a cross between the *217B:Gal4* and *UAS:YFP-NTR 2.0* transgenic lines that co-express YFP and NTR 2.0 in cells in the gut (YFP+). To ablate YFP-NTR 2.0 expressing cells, we treated YFP+ larvae with 400 µM MTZ for 24hrs (Sharrock et al., 2022) starting at 5 or 12 dpf. To assess the extent of ENS cell loss, we quantified YFP+ cells at 6 dpf and 13 dpf (1 dpt for MTZ-treated larvae). In untreated controls, no significant difference in YFP+ cells was observed between 5 and 6 dpf, or 12 and

297 13 dpf. Conversely, MTZ-treated groups showed a near-complete loss of YFP+ cell numbers at
298 1 dpt compared to 0 dpt (before treatment) and untreated control (**Figure 3**).
299 As 24 hrs of MTZ treatment showed robust YFP+ cell ablation at both developmental stages, we
300 decided to move forward with MTZ treatment at 12 dpf for further analyses. Embryonic
301 neurogenesis is still very active at 5 dpf (Olden et al., 2008; Roy-Carson et al., 2017). Therefore,
302 ablating neurons at 5 dpf might include processes of developmental neurogenesis rather than of
303 neuronal regeneration which we aimed to avoid.
304 To confirm that YFP+ cells are neurons at 12 dpf, we analyzed co-expression of YFP and
305 HuC/D in *217B:Gal4*; *UAS:YFP-NTR 2.0* fish. We found that 96.3% of YFP+ cells were also
306 HuC/D+ indicating that the vast majority of YFP+ cells are ENS neurons while only 3.7% YFP+
307 cells are HuC/D- (**Figure S2**). Therefore, we will hereafter refer to YFP+ cells in these lines as
308 YFP+ neurons. Based on total HuC/D+ numbers, our quantification also showed that YFP+
309 neurons comprise 22% of the total ENS neuronal population (data not shown).
310

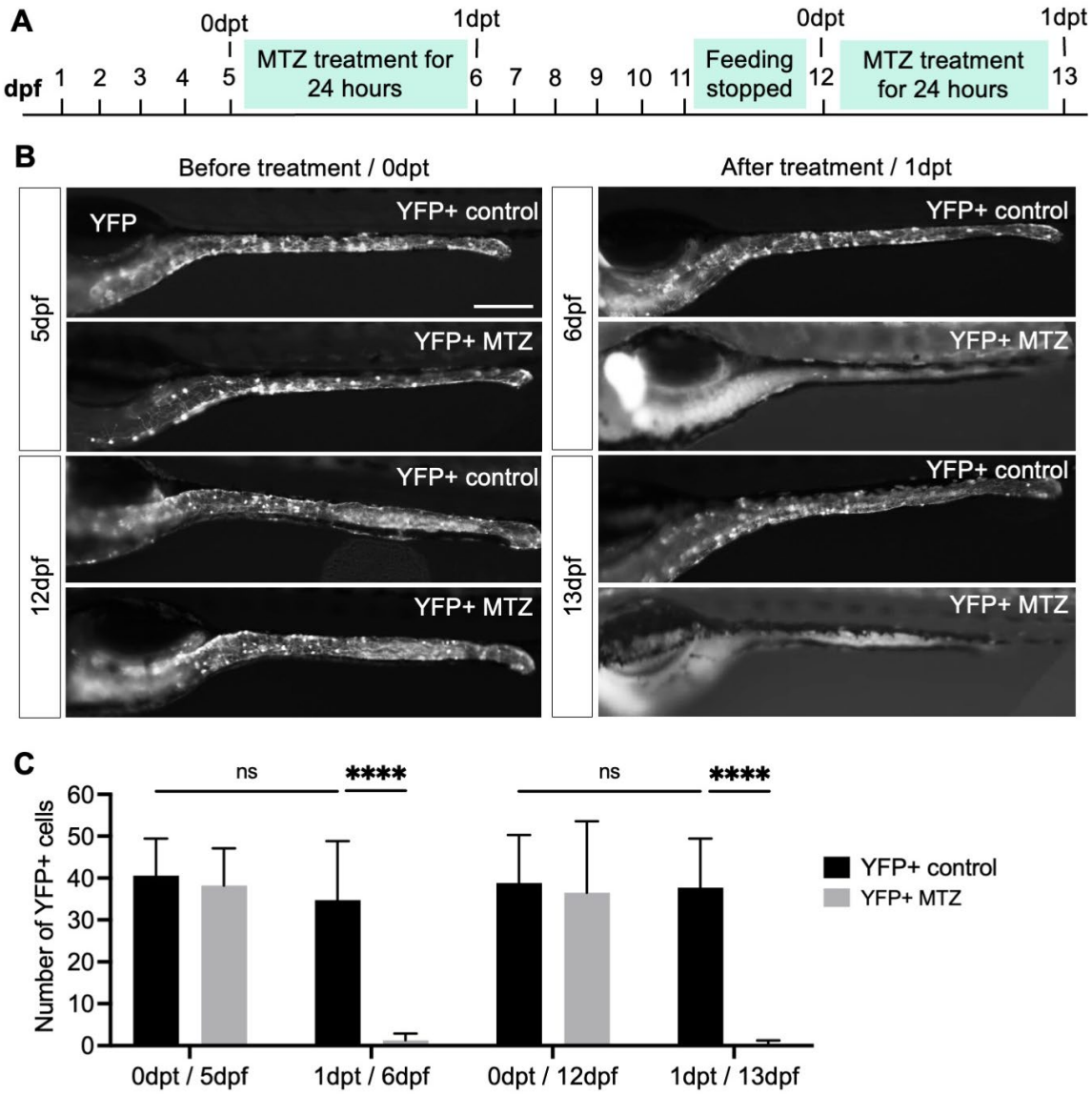

Figure 3. Establishment of a robust ENS neuron ablation assay. (A) The timeline of days post fertilization (dpf) and days post treatment (dpt) illustrates the experimental procedure for MTZ treatments initiated at either 5 or 12 dpf. **(B)** Whole-mount side views of live larval guts at the stage indicated. Left panel: YFP+ neurons (white dots) are present before treatment (0 dpt) at 5 or 12 dpf in YFP+ larvae. Right panel: after 24 h treatment with 400 μM Metronidazole (MTZ), YFP+ cells are completely absent in MTZ-treated fish (YFP+ MTZ) but present in untreated controls (YFP+ control). **(C)** Quantification of YFP+ neurons in control and MTZ-treated groups (n = 10 larvae per group, 2 experiments). Scale bar = 100 μm; Data are shown as mean ± SD. Statistical significance ****$p < 0.0001$.

312 **YFP+ neurons undergo DNA-damage induced cell death after MTZ treatment**
313 To test if YFP+ neurons undergo cell death after MTZ treatment, we evaluated changes in
314 neuronal morphology and performed TUNEL assay to detect cells undergoing cell death. YFP+
315 neurons in untreated control larvae displayed normal morphology with no visible signs of
316 morphological changes (**Figure 4A**). In contrast, YFP+ neurons in MTZ-treated samples
317 exhibited significant morphological changes, including axonal and cell body fragmentation and
318 retraction of neuronal processes, consistent with neurons undergoing cell death {**Figure 4**,
319 (Cusack et al., 2014)}. Additionally, we conducted TUNEL assays combined with
320 immunostaining for YFP to assess DNA damage in control and MTZ-treated fish at 6 hours post
321 treatment (hpt). As expected, we found GFP+/TUNEL+ cells both treated and control groups
322 since apoptotic cell death is a natural ongoing process at 12 dpf (Lee et al., 2023). However,
323 significantly higher number of GFP+/TUNEL+ cells were observed in the MTZ-treated group
324 compared to YFP+ untreated control (**Figure 4B, C**). In addition, GFP+/TUNEL+ neurons
325 exhibited clear morphological changes indicating that these neurons were undergoing cell death
326 (**Figure 4D**). These results indicate that MTZ treatment induces DNA damage which leads to
327 cell death with pronounced structural alterations attending this process.

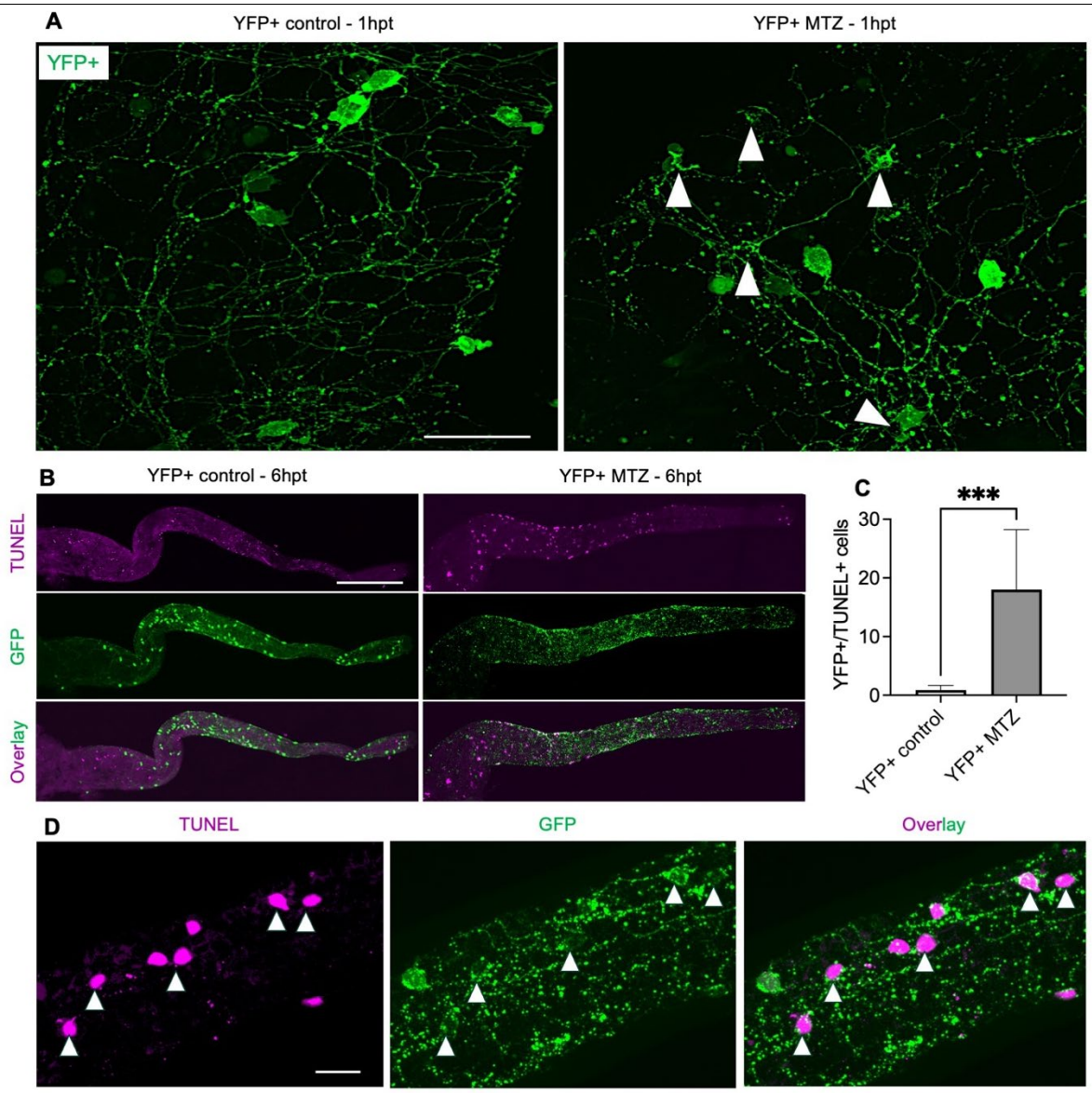

Figure 4. MTZ treatment induces DNA-damage cell death in YFP+ neurons. (A) In 12 dpf larvae, YFP+ neurons displays normal neuronal morphology in the untreated control group, while MTZ treated YFP+ neurons show fragmented and retracted neuronal processes at 1 hpt (white arrowheads; n=6 larvae per group, 2 experiments). **(B)** At 6 hpt, there is an increase in TUNEL staining (magenta) in YFP+ neurons (anti-GFP immunostaining) in MTZ treated larvae compared to untreated controls. In YFP+ control group, GFP+ neurons have normal morphology. In contrast, GFP+ neurons in the MTZ-treated group show fragmented morphology indicative of cell death. **(C)** Quantification of GFP+/TUNEL+ cells shows significant increase in YFP+ MTZ-treated larvae compared to YFP+ untreated control (n= 9 larvae per group, 2 experiments). **(D)** Magnified images of

GFP+/TUNEL+ cells (white arrowhead) in the YFP+ MTZ-treated group. (A-D) Maximum projection confocal images of dissected intestines at 1 hpt (A) and 6 hpt (B, D). Scale bars = 20 μm in A; 100 μm in B; 40 μm in D; Statistical significance: ***$p < 0.001$; dpf = days post fertilization; hpt = hours post treatment.

YFP+ neurons regenerate following targeted ablation

Next, we investigated whether YFP+ neuron numbers were restored to control levels, which would indicate that they regenerate after MTZ treatment. We quantified YFP+ neuron along the whole gut at different time points before and after treatment in YFP+ MTZ and YFP+ control larvae. YFP+ control larvae exhibited an obvious neuronal network from 0 to 15 dpt (**Figure 5A-B**). In contrast, YFP+ neuronal numbers were reduced in the YFP+ MTZ larvae at 1 dpt, confirming successful ablation of YFP+ neurons (**Figure 5A-B**). By 2 dpt, we find a small number of YFP+ neurons along with developing neurites that bridge across the gut (**Figure S3**). YFP+ neuron numbers continue to increase, but through 6 dpt there was a significant difference in YFP+ numbers compared to the control group. By 9 dpt, regenerated YFP+ neuron numbers reached levels comparable to the controls and remained at control levels through 12 and 15 dpt (**Figure 5A-B**). We noticed that approximately half of the YFP+ MTZ larvae exhibited abnormal body posture after 9 dpt. To investigate whether this affected YFP+ neuron regeneration, we compared regenerated YFP+ neuron counts in larvae with normal posture and those with defective posture at 12 dpt but found no significant difference (**Figure S4**). This indicates that postural defects did not impact neuron regeneration. To determine if there were differences in the timeline of neuron regeneration within discrete gut regions compared to the whole gut, we quantified YFP+ neurons in three main gut regions - anterior, midgut, and posterior (Jianlong Li et al., 2024; Wallace et al., 2005). We found that the timeline of YFP+ neuron regeneration was the same in the three gut regions as in the whole gut (**Figure 5C, B-F**).

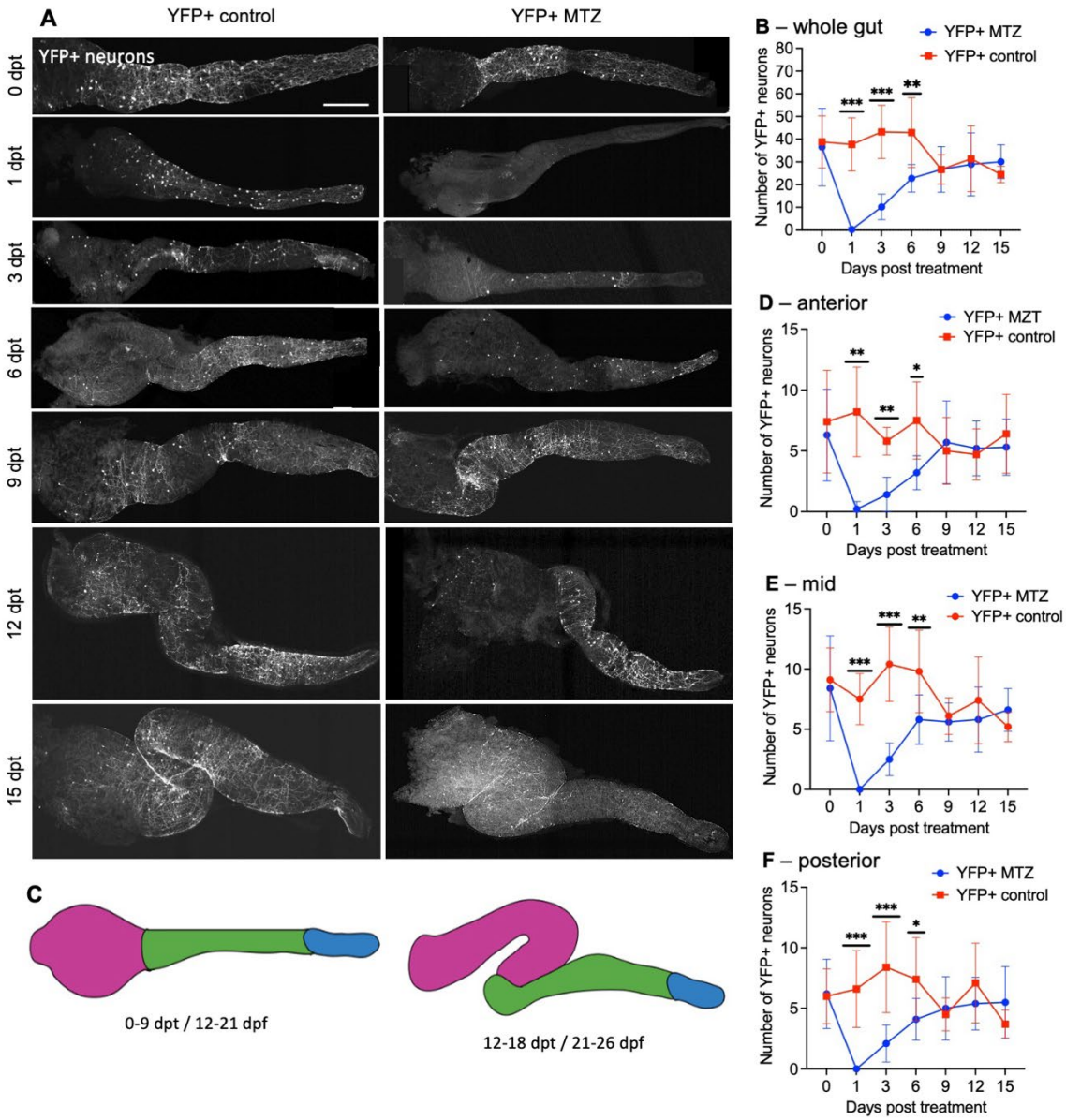

Figure 5. Timeline of YFP+ neuron regeneration in the whole intestine and defined gut regions.

(A) YFP+ neurons (labelled with anti-GFP antibody) and the neuronal network in YFP+ control and YFP+ MTZ zebrafish larvae at 0 (before treatment) and 1, 3, 6, 9, 12, and 15 dpt. **(B)** YFP+ control larvae exhibited consistent GFP+ neuron numbers till 6 dpt with a slight decrease by 9 through 15 dpt. In contrast, the YFP+ MTZ group showed a dramatic decrease in YFP+ neurons, confirming complete ablation of YFP+ neurons ($p < 0.001$) at 1 dpt. A small number of YFP+ neurons appeared by 3 and 6 dpt, but YFP+ neuron numbers were still significantly decreased compared to the control. By 9 dpt, neuronal number fully recovered

with no significant difference between treated and controls at 9, 12 and 15 dpt. **(C)** Schematic representation of the zebrafish gut regions shows the three analyzed gut regions (magenta = anterior, green = midgut, blue = posterior) at 0–9 dpt and 12–18 dpt based on Jianlong Li et al. (2024) and Wallace et al. (2005). Anterior **(D)**, mid **(E)** and posterior **(F)** gut regions show the same timeline of YFP+ neuron regeneration as the whole gut **(B)**. **(A)** Maximum projection confocal images of dissected intestines at time point indicated; Scale bar = 100 µm; Data are presented as mean ± SD (10 larvae per group, 2 experiments); Statistical significance: ***$p < 0.001$, **$p < 0.01$ and *$p < 0.05$; dpt = days post treatment

351

352 **Effect of YFP+ neuron ablation on other ENS neurons**

353 As shown before, YFP+ neurons colocalized with a small subset of HuC/D+ neurons, indicating
354 that only a fraction of ENS neurons were ablated (**Figure 6A, B, S2**). To assess if ablation of
355 YFP+ neurons has any effects on the YFP- ENS neuronal population, we quantified HuC/D+
356 neurons in YFP+ MTZ and YFP+ control groups at 0 dpt (before treatment) and 1dpt (**Figure 6**).
357 We found no significant difference in HuC/D+ neuron numbers between treated and control
358 groups after ablation of YFP+ neuron (**Figure 6C**). This lack of significance may be due to the
359 relatively small proportion of YFP+ neurons within the total HuC/D+ population - approximately
360 40 out of 300 neurons. Additionally, MTZ treatment alone in YFP- MTZ treated larvae did not
361 significantly decrease overall HuC/D numbers (**Figure S5**).

362

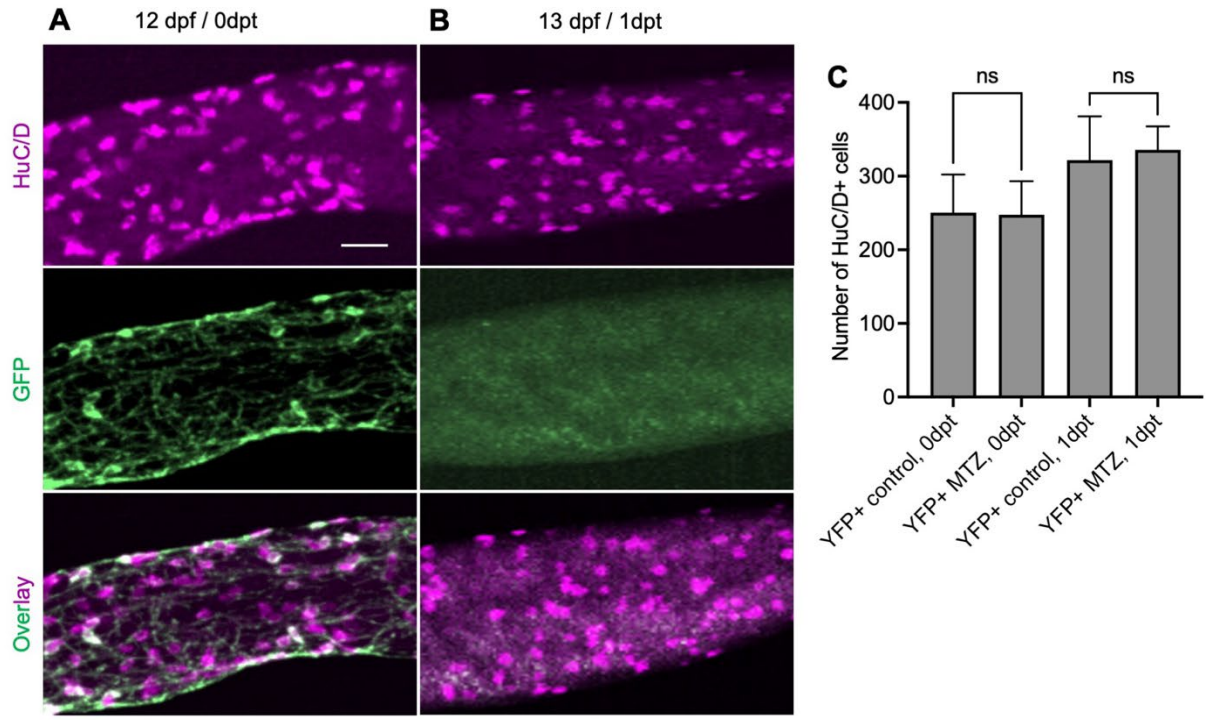

Figure 6. YFP+ neuron loss does not significantly affect YFP- enteric neuron numbers. **(A)** At 12 dpf (before treatment, 0 dpt), the pan-neuronal marker HuC/D (magenta) and YFP+ cells (labeled with anti-GFP, green) show high colocalization (overlay). **(B)** Following MTZ treatment at 13dpf (1dpt), GFP-HuC/D+ cells are present, whereas GFP+ cells are completely absent due to ablation of YFP+ neurons. **(C)** Quantification of HuC/D-positive neuron counts before (0 dpt) and after MTZ treatment (1dpt). There was no significant difference in total HuC/D+ cells between control and treatment group (n = 10 larvae per group, 2 experiments). **(A-B)** Maximum projection confocal images of dissected intestines. Scale bar = 100 µm; Data are presented as mean ± SD, ns = not significant; dpf = days post fertilization; dpt = days post treatment

363

364 **Specific co-expressed neuronal subtypes regenerate following ablation**

365 The ENS is composed of different neuron subtypes which control the different functions of the
366 gut including gut motility (Holmberg et al., 2006; Roach et al., 2013; Uyttebroek et al., 2010).
367 The main neuronal subtypes in the zebrafish ENS are nitrergic neurons (neuronal nitric oxide
368 synthase+ (nNOS+), serotonergic (5-hydroxytryptamine+ (5-HT+), vipergic (*vasoactive intestinal*
369 *peptide*+ (*vip*+), and cholinergic (*solute carrier family 18 member 3a*+ (*slc18a3a*+) neurons
370 (Uyttebroek et al., 2010). To determine the subtype composition within the YFP+ neuronal

371 population, we analyzed co-expression of these subtype markers with YFP at 12 dpf, prior to
372 MTZ treatment. At 0 dpt, we found that 57.54%, 12.26%, 13.33%, and 6.58% of YFP+ neurons
373 co-expressed nNOS, 5-HT, *vip*, and *slc18a3a*, respectively, indicating the presence of distinct
374 YFP+ neuronal subtypes prior to ablation (**Figure S6**).

375 To examine if all YFP+ expressing subtypes regenerated at 9 dpt, we analyzed the number of
376 YFP+/subtype+ neurons in the MTZ-treated group and compared them to untreated control and
377 baseline at 0 dpt control. Notably, the number of YFP+/nNOS+ neurons remained unchanged
378 between 0 control and 9 dpt control, and there was no significant difference between MTZ-
379 treated and control group, suggesting robust stability and regenerative capacity for
380 YFP+/nNOS+ neurons (**Figure 7A, B**). Analysis of YFP+/5-HT+ neurons revealed no significant
381 difference between 0 dpt control and the 9 dpt control group. However, in the MTZ-treated
382 group, the number of YFP+/5-HT+ neurons at 9 dpt remained significantly lower compared to
383 control, indicating a limited or delayed regenerative capacity for this neuronal subtype (**Figure**
384 **7C, D**).
385 Using HCR to detect *vip* and *slc18a3a* expression, we found that the number of YFP+/*vip*+
386 neurons significantly decreased within the control group between 0 and 9 dpt. However, no
387 significant difference was observed between the MTZ-treated and control groups at 9 dpt,
388 suggesting that YFP+/*vip*+ neurons had successfully regenerated by this time point (**Figure 8A,**
389 **B)**. Lastly, analysis of the cholinergic marker *slc18a3a* showed no significant differences across
390 groups, indicating that YFP+/*slc18a3a*+ neurons remained stable in the control group and were
391 successfully restored following regeneration (**Figure 8C, D**).

392 Overall, these findings suggest that the majority of YFP+ cells are nitrergic neurons before
393 ablation. After regeneration, YFP+/nNOS+, YFP+/*vip*+ and YFP+/*slc18a3a*+ neurons are
394 successfully restored. In contrast the YFP+/5-HT+ neurons exhibited lower and/or slower
395 regenerative capacity compared to the other subtypes.

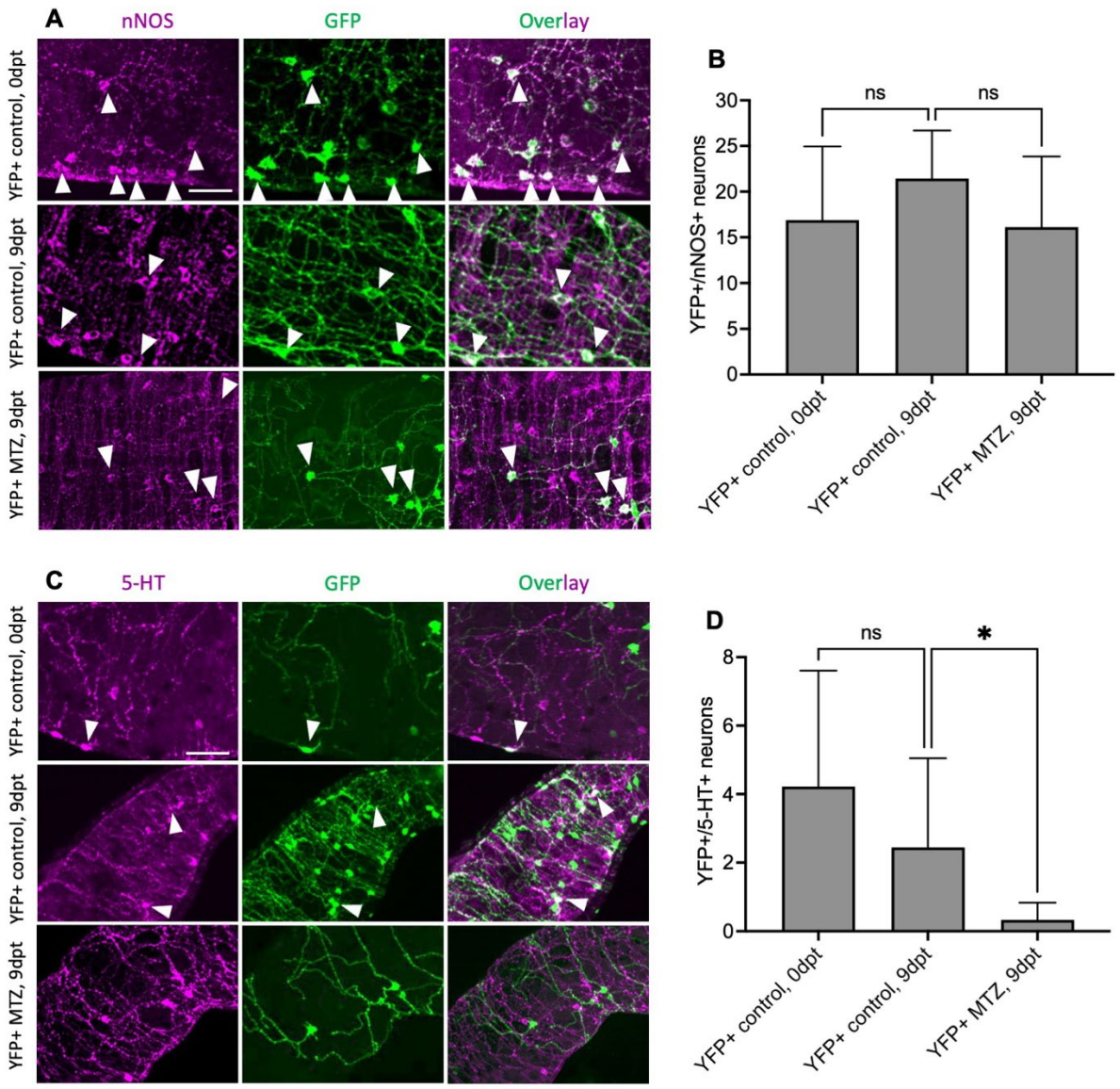

Figure 7: YFP+/nNOS+ but not YFP+/5-HT+ neurons regenerate following ablation. **(A)** Example of nNOS+ (magenta) and YFP+ (labeled with anti-GFP antibody, green) neurons that co-localize (overlay) at 0 dpt control (before treatment) and at 9 dpt in YFP+ control and YFP+ MTZ groups (white arrowheads). **(B)** Quantification of GFP+/nNOS+ neurons at 0 dpt control and 9 dpt in YFP+ control and YFP+ MTZ shows no significant difference (n = 10 larvae per group, 2 experiments). **(C)** Example of 5-HT (magenta) and YFP+ (labeled with anti-GFP antibody, green) neurons that co-localize (overlay) at 0 dpt control and 9 dpt in YFP+ control and YFP+ MTZ groups (white arrowheads). **(D)** Quantification of GFP+/5-HT+ at 0 dpt control and 9 dpt in YFP+ control and YFP+ MTZ. There is no significant difference between 0 dpt and 9 dpt in the YFP+ control group, but GFP+/5-HT+ neurons are significantly

reduced in in the MTZ-treated group compared to the control group at 9 dpt (n = 10 larvae per group, 2 experiments). **(A, C)** Maximum projection confocal images of dissected intestines at stage indicated; Scale bars = 10 μm; Data are presented as mean ± SD; Statistical significance: ***$p < 0.001$ and *$p < 0.05$; ns = non-significant difference; dpt = days post treatment.

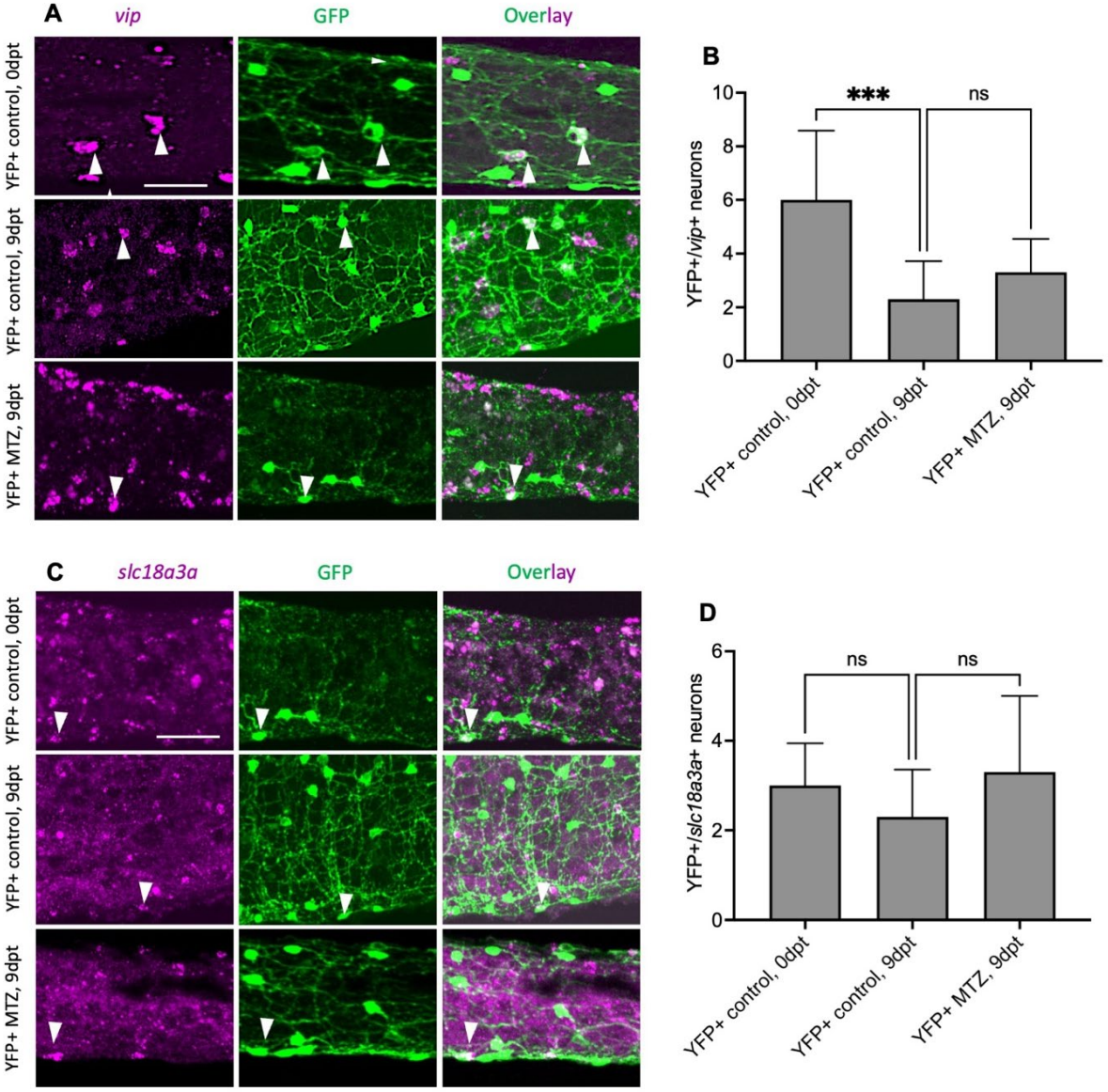

Figure 8. YFP+/*vip*+ and YFP+/*slc18a3a*+ neuron regenerate following ablation.
(A) Example of *vip* (magenta) and YFP+ (labeled with anti-GFP antibody, green) neurons that co-localize (overlay) at 0 dpt control (before treatment), and 9 dpt in YFP+ control and YFP+ MTZ (white arrowheads). **(B)** Quantification of GFP+/*vip*+ neuron at 0 dpt control and 9 dpt in both YFP+ control and YFP+ MTZ groups. A significant difference is observed between 0 dpt

and 9 dpt control groups. However, there is no significant difference between 9 dpt control and MTZ-treated groups (n = 10 larvae per group, 2 experiments). **(C)** Example of *slc18a3a* (magenta) and YFP+ (labeled with anti-GFP antibody, green) neurons that co-localize (overlay) at 0 dpt control and 9 dpt of YFP+ control and YFP+ MTZ (white arrowheads). **(D)** Quantification of GFP+/*slc18a3a*+ neurons shows no significant difference between the groups (n = 10 larvae per group, 2 experiments). **(A, C)** Maximum projection confocal images at stage indicated. Scale bars = 10 μm; Data are presented as mean ± SD; Statistical significance: ***$p < 0.001$ and **$p < 0.01$; ns = non-significant difference; dpt = days post treatment.

396

397 **Decreased gut wave movements recover to control levels after neuronal regeneration**

398 ENS neurons play a critical role in regulating gut motility (Furness, 2012; Kunze & Furness, 1999),
399 thus, we aimed to determine i) whether the loss of YFP+ neurons affects gut motility and ii) whether
400 the regenerated neurons restore gut function lost after ablation. To assess this, we examined one
401 measure of gut motility, the time of the Peristaltic Wave Interval (PWI) of anterograde movements
402 (Holmberg et al., 2006). We measured the PWI at three different time points at 1 dpt, 3 dpt and 9 dpt
403 in YFP+ and YFP- MTZ treated fish, and YFP+ untreated controls. We included the YFP- MTZ
404 treated group to determine if MTZ treatment alone impacted PWI. At 1 dpt, we found no significant
405 difference in the PWI time between control and treated groups (**Figure 9A, Supplementary Videos**
406 **S1-3**). However, at 3 dpt, the PWI time in the YFP+ MTZ treated group increased significantly
407 compared to both control groups, suggesting slower peristaltic movement in the YFP+ MTZ group
408 (**Figure 9B, supplementary videos S4-6**). At 9 dpt, the PWI time in the YFP+ MTZ treated group
409 was back to control levels (**Figure 9C, supplementary videos S7-9**). Overall, our results suggest
410 that gut motility function is affected after YFP+ neuronal loss and then restored after regeneration,
411 indicating functional recovery.

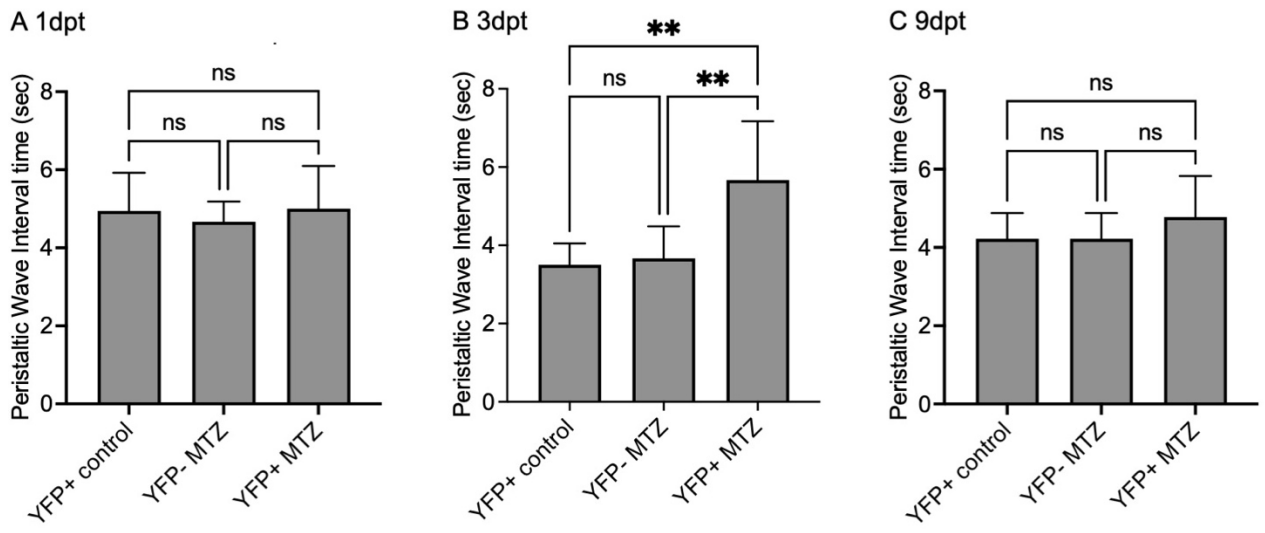

Figure 9. Peristaltic Interval Wave time recovers at 9 dpt after YFP+ neuron ablation. (A) At 1 dpt, there is no significant difference in gut PWI time across all experimental groups, YFP+ MTZ treated, YFP+ untreated control, YFP- MTZ treated. **(B)** At 3 dpt, YFP+MTZ treated larvae showed significantly slower gut PWI time compared to both control groups. **(C)** At 9 dpt, there was no significant difference in PWI across all experimental groups. Data are presented as mean ± SD (n = 6 larvae per group, 2 experiments). Statistical significance is indicated as $^{**}p < 0.01$, ns = non-significant. dpt = days post treatment.

Discussion

The topic of reparative regeneration has gained significant attention the past decade due to its potential therapeutic implications, for example to treat ENS diseases with loss of ENS neurons. Yet, to date, no study has demonstrated functional ENS neuron regeneration either in mammalian models or in zebrafish. In the present study, we show targeted ablation and functional regeneration of ENS neurons for the first time in zebrafish (**Figure 10**). Our results determined the spatial and temporal dynamics of targeted neuron loss as demonstrated by TUNEL assays and the recovery of ablated neuron numbers by 9 dpt of the majority on ENS neuron subtypes investigated. Specifically, among the regenerated neurons, we found full recovery of nitrergic, cholinergic, and vipergic subtypes. Importantly, we also showed functional impacts of neuronal ablation on a gut motility parameter and its full functional recovery suggesting functional regeneration in our system (**Figure 10**).

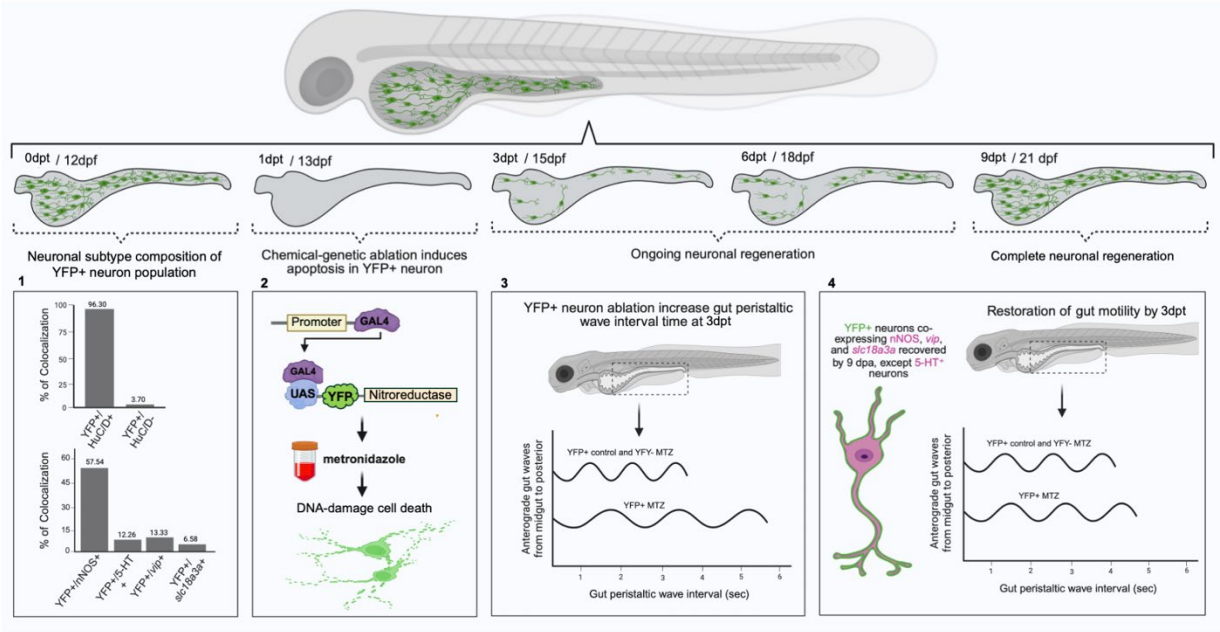

Figure 10. Timeline of events after targeted ablation and regeneration of ENS neurons in zebrafish. Timeline from 0 dpt / 12 dpf to 9 dpt / 21 dpf depicts the different events: i) Neuronal subtype composition of YFP+ neuron population at 0 dpt; ii) Chemical-genetic ablation approach activates cell death of YFP+ neurons to completely ablate YFP+ neurons; iii) neuronal regeneration at 3 and 6 dpt which affects gut peristalsis at 3 dpt; iv) complete regeneration of YFP+ cells and functional recovery at 9 dpt. **Panel 1** (0 dpt / 12 dpf): YFP+ cells co-localize with the pan-neuronal marker HuC/D and various neuronal subtypes (nNOS, 5-HT, *vip*, and *slc18a31a*). **Panel 2** (1 dpt / 13 dpf): Set-up of Gal4-UAS:NTR 2.0 based ablation system. MTZ treatment induces DNA-damage cell death in YFP+ neurons as confirmed by TUNEL assay. **Panel 3** (3 dpt / 15 dpf): Neuronal ablation resulted in increased peristaltic wave interval time, reflecting reduced gut motility. **Panel 4** (9 dpt / 21 dpf): Complete recovery of YFP+ neurons and most neuronal subtypes (nNOS+, *vip*+, *slc18a31*+), except 5-HT+ neurons and full functional recovery of gut motility. dpf = days post fertilization, dpt = days post treatment.

425

426 **Extensive ENS neuron ablation and their complete regeneration in zebrafish**

427 In zebrafish, the only two studies to study ENS neurons regeneration used laser ablation to target
428 few ENS neurons in a small gut region. Both studies reported generation of new neurons following
429 ablation (El-Nachef & Bronner, 2020, Ohno et al., 2021). However, quantification of regenerated

neurons showed that they did not return to control levels in the analyzed time frame, nor were impacts of gut function investigated (Ohno et al., 2021). In our study, we find robust regeneration of ablated cells to control levels by 9 dpt which stay at control levels through 15 dpt, the last time point that we analyzed. We find that different neuronal subtypes are able to regenerate but identify interesting subtype-specific differences in regenerative capacity or timing (**Figure 10**). Our work also shows for the first time recovery of a parameter of gut function - gut wave propagation - indicative of successful functional regeneration (**Figure 10**). In addition, our approach has several experimental advantages compared to laser ablation. First, laser ablation is less efficient, as it can only ablate a limited number of neurons within specific gut regions (El-Nachef & Bronner, 2020, Ohno et al., 2021). For instance, one study only ablated ~16 neurons within one-somite-width of the posterior gut at 10-15 dpf (Ohno et al., 2021). In contrast, our genetic chemical ablation system successfully ablated on average 44 neurons throughout the whole gut, significantly improving efficiency. Second, laser ablation is time-consuming as it requires individual larval preparation and precise manual targeting (Ohno et al., 2021). In contrast, our methods enable the simultaneous ablation of ENS neurons in several hundred of larvae. Third, laser irradiation can cause unintended damage to non-neuronal, surrounding tissues, including smooth muscle and epithelial cells, which may impact regeneration and complicate downstream analyses such as gut motility. In contrast, our approach is spatiotemporally controlled ablation that precisely targets only specific ENS neurons and had no deleterious effects on the overall neuronal population in the gut (**Figure 10**).

Zebrafish are a powerful model system to study ENS regeneration

So far, ENS regeneration research has mostly focused on mammalian model systems with only limited work in non-mammalian models such as zebrafish (Corvetti et al., 2001; El-Nachef & Bronner, 2020; Gabella & Trigg, 1984; Galligan et al., 1989; Hanani et al., 2003; Jew et al., 1989; Joseph et al., 2011; Karaosmanoğlu et al., 1996; Laranjeira et al., 2011; Luck et al., 1993; Ohno et al., 2021; Stavely et al., 2024; Tokui et al., 1994). Previous studies in mammalian models involving surgical (Galligan et al., 1989; Karaosmanoğlu et al., 1996; Tokui et al., 1994), stenosis (Corvetti et al., 2001; Gabella & Trigg, 1984; Jew et al., 1989; Joseph et al., 2011), and chemical (Hanani et al., 2003; Laranjeira et al., 2011; Luck et al., 1993) ablation methods consistently report incomplete neuronal regeneration, and gut region- or species-specific differences in regenerative outcomes of ENS neurons (Rueckert and Ganz, 2022). Notably, all previous approaches also reported structural abnormalities at the injury site by co-lateral damage of surrounding tissues. To addresses this, recent works in adult mice reported focal ablation specifically of ENS neurons using a chemical-genetic ablation approach (Bhave et al., 2019; Stavely et al., 2024). Even though this study reported

463 that mature, post-mitotic enteric neurons in adult mice can regenerate axons and reinnervate the gut
464 after injury, there was still limited regeneration of neurons even three months after ablation (Stavely
465 et al., 2024). This indicates that mammals have limited ENS regenerative abilities which may be due
466 to lack of signals or progenitor cells that enable full neuronal regeneration.

467 In contrast, the present study demonstrates that zebrafish are a powerful model to study the signals
468 and cellular-molecular processes underlying functional ENS regeneration. Our spatio-temporally
469 controlled approach ablates approximately one fifth of all ENS neurons by inducing cell death with
470 subsequent full recovery after only 9 days. Ablation along the entire gut will enable the analysis of
471 cellular responses and gene regulatory programs active during ENS regeneration as whole guts can
472 be analyzed. This approach thus provides a rapid experimental setup to identify the signals and
473 cellular responses important for neuronal regeneration in the ENS in the future (**Figure 10**).

474 **Regeneration of neurons in the zebrafish CNS *vs* ENS**

475 The zebrafish central nervous system has been extensively studied with regards to its regenerative
476 capacity (Kaslin et al., 2009, 2013; März et al., 2010) while little is known about ENS regeneration
477 (Ohno et al., 2021). In the central nervous system, brain regions show different capacities to
478 regenerate neuronal subtypes. In the zebrafish telencephalon, all ablated neuron types regenerate
479 (Barbosa et al., 2015; Kroehne et al., 2011; Reimer et al., 2008), whereas the cerebellum is capable
480 of regenerating many, but not all neuron types (Kaslin et al., 2017). This variable regenerative
481 capacity of the cerebellum has been attributed to varying ability of cerebellar stem and progenitor
482 cells to generate neurons and glia throughout the lifespan (Kaslin et al., 2009, 2013). We also find
483 differences in regeneration of neuron types in the ENS where some subtypes (nitrergic, cholinergic
484 and vipergic) regenerate fully, whereas serotonergic neurons do not reach control levels (**Figure**
485 **10**). There could be two possibilities for this difference in regeneration: (1) serotonergic neurons take
486 longer to regenerate, (2) the progenitor cells or cellular mechanisms to regenerate serotonergic
487 neurons are not activated at this stage of post-embryonic development. Further work will determine
488 which cellular responses are triggered after cell ablation and the progenitor population(s) that
489 generate new ENS neurons and neuronal subtypes in zebrafish.

490 **Supplementary Materials**

491 The following supporting information can be downloaded at: https:

492

493 **Author Contributions**

494 Conceptualization: M.A.S, K.K. M., H.R., J.G. Methodology, Data curation, Validation, Formal
495 Analysis and Investigation: M.A.S, K.K. M., H.R. Visualization: M.A.S. Writing—Original Draft

Preparation: M.A.S. Writing—Review and Editing: M.A.S, K.K. M., H.R., A.V.S., D.F.A., J.S.M., and J.G. Supervision, Project Administration, Funding Acquisition and Recourses: D.F.A., J.S.M., J.G. All authors have read and agreed to the published version of the manuscript.

Funding:

This work was supported by NSF CAREER #2143267 to J.G., NIH R21NS123629 to J.G., and a Research Grant from the American Neurogastroenterology and Motility Society to J.G. NIH R01OD020376 to J.S.M. and D.F.A., supported development of the improved NTR 2.0 enzyme.

Institutional Review Board Statement:

The animal study protocol was approved by the Michigan State University Institutional Animal Care and Use Committee

Acknowledgments

We want to thank Rachel Alcorn, Taylor Lawrence, Giovanna Haddock, Kristen Lounsbury, Anthony Turner, and Samantha Lampman for excellent fish care.

Conflicts of Interest

The authors declare no competing or financial interests

List of Abbreviations

ENS = Enteric nervous system
MTZ = Metronidazole
HSCR = Hirschsprung Disease
DPF = Days post fertilization
DPT = Days post treatment
HPT = Hours post treatment
NTR = Nitroreductase
YFP = Yellow fluorescent protein
GFP = Green fluorescent protein
UAS = Upstream activating sequence
PWI = Peristaltic Wave Interval
TdT = Terminal deoxynucleotidyl Transferase
BSA = Bovin serum albumin

PBS = Phosphate-Buffered Saline

HCR = Hybridization Chain Reaction

References

Ariga, J., Walker, S. L., & Mumm, J. S. (2010). Multicolor time-lapse imaging of transgenic zebrafish: Visualizing retinal stem cells activated by targeted neuronal cell ablation. *Journal of Visualized Experiments*, *(43):2093*. https://doi.org/10.3791/2093

Asakawa, K., Suster, M. L., Mizusawa, K., Nagayoshi, S., Kotani, T., Urasaki, A., Kishimoto, Y., Hibi, M., & Kawakami, K. (2008). Genetic dissection of neural circuits by Tol2 transposon-mediated Gal4 gene and enhancer trapping in zebrafish. *Proceedings of the National Academy of Sciences of the United States of America*, *105*(4), 1255–1260. https://doi.org/10.1073/pnas.0704963105

Bandla, A., Melancon, E., Taylor, C. R., Davidson, A. E., Eisen, J. S., & Ganz, J. (2022). A New Transgenic Tool to Study the Ret Signaling Pathway in the Enteric Nervous System. *International Journal of Molecular Sciences*, *23*(24). https://doi.org/10.3390/ijms232415667

Barbosa, J. S., Sanchez-Gonzalez, R., Di Giaimo, R., Baumgart, E. V., Theis, F. J., Götz, M., & Ninkovic, J. (2015). Live imaging of adult neural stem cell behavior in the intact and injured zebrafish brain. *Science*, *348*(6236), 789–793. https://doi.org/10.1126/science.aaa2729

Bhave, S., Arciero, E., Baker, C., Ho, W. L., Stavely, R., Goldstein, A. M., & Hotta, R. (2019). Enteric neuronal cell therapy reverses architectural changes in a novel diphtheria toxin-mediated model of colonic aganglionosis. *Scientific Reports*, *9*(18756). https://doi.org/10.1038/s41598-019-55128-4

Bridgewater, J. A., Springer, C. J., Knox, R. J., Minton, N. P., Michael, N. P., & Collins, M. K. (1995). Expression of the bacterial nitroreductase enzyme in mammalian cells renders them selectively sensitive to killing by the prodrug CB1954. *European Journal of Cancer*, *31*(13–14), 2362–2370. https://doi.org/10.1016/0959-8049(95)00436-X

Burns, A. J., Goldstein, A. M., Newgreen, D. F., Stamp, L., Metzger, M., Hotta, R., Young, H. M., Andrews, P. W., Belkind-gerson, J., Bondurand, N., Bornstein, J. C., Yee, W., Cheah, K., Gershon, M. D., Heuckeroth, R. O., Robert, M. W., Just, L., Kapur, R. P., King, S. K., … Urology, P. (2016). *HHS Public Access*. *417*(2), 229–251. https://doi.org/10.1016/j.ydbio.2016.04.001

Butler Tjaden, N. E., & Trainor, P. A. (2013). The developmental etiology and pathogenesis of Hirschsprung disease. *Translational Research*, *162*(1), 1–15. https://doi.org/10.1016/j.trsl.2013.03.001

Cao, J., & Poss, K. D. (2018). The epicardium as a hub for heart regeneration. In *Nature Reviews Cardiology*. 15, pages 631–647. https://doi.org/10.1038/s41569-018-0046-4

573 Corvetti, G., Fornaro, M., Geuna, S., Poncino, A., & Giacobini-Robecchi, M. G. (2001).
574 Unscheduled DNA synthesis in rat adult myenteric neurons: An
575 immunohistochemical study. *NeuroReport*, *12*(10), 2165–2168.
576 https://doi.org/10.1097/00001756-200107200-00024
577 Cusack, C. L., Swahari, V., Henley, W. H., Ramsey, J. M., & Deshmukh, M. (2013).
578 Distinct Pathways Mediate Axon Degeneration during Apoptosis and Axon-Specific
579 Pruning. *Nature communications*. *4: 1876.* doi:10.1038/ncomms2910
580 Davison, J. M., Akitake, C. M., Goll, M. G., Rhee, J. M., Gosse, N., Baier, H., Halpern,
581 M. E., Leach, S. D., & Parsons, M. J. (2007). Transactivation from Gal4-VP16
582 transgenic insertions for tissue-specific cell labeling and ablation in zebrafish.
583 *Developmental Biology*, *304*(2), 811–824.
584 https://doi.org/10.1016/j.ydbio.2007.01.033
585 Elmonem, M. A., Berlingerio, S. P., van den Heuvel, L. P., de Witte, P. A., Lowe, M., &
586 Levtchenko, E. N. (2018). Genetic renal diseases: The emerging role of zebrafish
587 models. *Cells*. *7*(9). https://doi.org/10.3390/cells7090130
588 El-Nachef, W. N., & Bronner, M. E. (2020). De novo enteric neurogenesis in post-
589 embryonic zebrafish from Schwann cell precursors rather than resident cell types.
590 *Development (Cambridge)*, *147*(13), dev186619.
591 https://doi.org/10.1242/dev.186619
592 Furness, J. B. (2012). The enteric nervous system and neurogastroenterology. *Nature*
593 *Reviews Gastroenterology and Hepatology*, *9*(5), 286–294.
594 https://doi.org/10.1038/nrgastro.2012.32
595 Gabella, G., & Trigg, P. (1984). Size of neurons and glial cells in the enteric ganglia of
596 mice, guinea-pigs, rabbits and sheep. *Journal of Neurocytology*, *13*(1), 49–71.
597 https://doi.org/10.1007/BF01148318
598 Galligan, J. J., Furness, J. B., & Costa, M. (1989). Migration of the myoelectric complex
599 after interruption of the myenteric plexus: Intestinal transection and regeneration of
600 enteric nerves in the guinea pig. *Gastroenterology*, *97*(5), 1135–1146.
601 https://doi.org/10.1016/0016-5085(89)91683-1
602 Ganz, J. (2018). Gut feelings: Studying enteric nervous system development, function,
603 and disease in the zebrafish model system. *Developmental Dynamics*, *247*(2),
604 268–278. https://doi.org/10.1002/dvdy.24597
605 Hanani, M., Ledder, O., Yutkin, V., Abu-Dalu, R., Huang, T. Y., Härtig, W., Vannucchi,
606 M. G., & Faussone-Pellegrini, M. S. (2003). Regeneration of myenteric plexus in
607 the mouse colon after experimental denervation with benzalkonium chloride.
608 *Journal of Comparative Neurology*, *462*(3), 315–327.
609 https://doi.org/10.1002/cne.10721
610 Hanovice, N. J., Leach, L. L., Slater, K., Gabriel, A. E., Romanovicz, D., Shao, E.,
611 Collery, R., Burton, E. A., Lathrop, K. L., Link, B. A., & Gross, J. M. (2019).
612 Regeneration of the zebrafish retinal pigment epithelium after widespread genetic
613 ablation. *PLoS Genetics* 15 (1). https://doi.org/10.1371/journal.pgen.1007939
614 Hao, M. M., & Young, H. M. (2009). Development of enteric neuron diversity. *Journal of*
615 *Cellular and Molecular Medicine*, *13*(7), 1193–1210. https://doi.org/10.1111/j.1582-
616 4934.2009.00813.x
617 Heanue, T. A., Boesmans, W., Bell, D. M., Kawakami, K., Berghe, P. Vanden, &
618 Pachnis, V. (2016). A Novel Zebrafish ret Heterozygous Model of Hirschsprung

619 Disease Identifies a Functional Role for mapk10 as a Modifier of Enteric Nervous
620 System Phenotype Severity. 30;12(11):e1006439. https://doi:
621 10.1371/journal.pgen.1006439. eCollection 2016 Nov
622 Holmberg, A., Olsson, C., & Holmgren, S. (2006). The effects of endogenous and
623 exogenous nitric oxide on gut motility in zebrafish Danio rerio embryos and larvae.
624 *Journal of Experimental Biology*, *209*(13), 2472–2479.
625 https://doi.org/10.1242/jeb.02272
626 Howe, K., Clark, M. D., Torroja, C. F., Torrance, J., Berthelot, C., & Muffato, M. (2013).
627 The zebrafish reference genome sequence and its relationship to the human
628 genome. *Nature*, *496*(7446), 598–503. https://doi.org/10.1038/nature12111
629 Ibarra-García-Padilla, R., Howard, A. G. A., Singleton, E. W., & Uribe, R. A. (2021). A
630 protocol for whole-mount immuno-coupled hybridization chain reaction (WICHCR)
631 in zebrafish embryos and larvae. *STAR Protocols*, *2*(3).
632 https://doi.org/10.1016/j.xpro.2021.100709
633 Jew, J. Y., Zhang, M. Q., Williams, T. H., & Gabella, G. (1989). The Intestine as a Model
634 for Neuronal Plasticity. *Archives of Histology and Cytology*, *52*, 167–180.
635 https://doi.org/10.1679/aohc.52.Suppl_167
636 Jianlong Li, Prochaska, M., Maney, L., & Wallace, K. N. (2024). Development and
637 organization of the zebrafish intestinal epithelial stem cell niche. *Development*
638 *Dynamics*, *249(1),76-87. doi: 10.1002/dvdy.16. Epub 2019 Feb 18*
639 Joseph, N. M., He, S., Quintana, E., Kim, Y. G., Núñez, G., & Morrison, S. J. (2011).
640 Enteric glia are multipotent in culture but primarily form glia in the adult rodent gut.
641 *Journal of Clinical Investigation*, *121*(9), 3398–3411.
642 https://doi.org/10.1172/JCI58186
643 Karaosmanoğlu, T., Müftüoğlu, S., Dağdeviren, A., Durgun, B., Aygün, B., & Örs, Ü.
644 (1996). Morphological changes in the myenteric plexus of rat ileum after transection
645 and end-to-end anastomosis. *Journal of Anatomy*, *188*, 323–331.
646 Kaslin, J., Ganz, J., Geffarth, M., Grandel, H., Hans, S., & Brand, M. (2009). Stem cells
647 in the adult zebrafish cerebellum: Initiation and maintenance of a novel stem cell
648 niche. *Journal of Neuroscience*, *29*(19), 6142–6153.
649 https://doi.org/10.1523/JNEUROSCI.0072-09.2009
650 Kaslin, J., Kroehne, V., Benato, F., Argenton, F., & Brand, M. (2013). Development and
651 specification of cerebellar stem and progenitor cells in zebrafish: From embryo to
652 adult. *Neural Development*, *8*(1). https://doi.org/10.1186/1749-8104-8-9
653 Kaslin, J., Kroehne, V., Ganz, J., Hans, S., Brand, M., Kaslin, J., Kroehne, V., Ganz, J.,
654 Hans, S., & Brand, M. (2017). Correction to: Distinct roles of neuroepithelial-like
655 and radial glia-like progenitor cells in cerebellar regeneration. *Development*,
656 *144*(18), 3388. https://doi.org/10.1242/dev.158600
657 Kawakami, K., Abe, G., Asada, T., Asakawa, K., Fukuda, R., Ito, A., Lal, P., Mouri, N.,
658 Muto, A., Suster, M. L., Takakubo, H., Urasaki, A., Wada, H., & Yoshida, M. (2010).
659 ZTrap: Zebrafish gene trap and enhancer trap database. *BMC Developmental*
660 *Biology*, *10*. https://doi.org/10.1186/1471-213X-10-105
661 Kimmel CB, Ballard WW, Kimmel SR, Ullmann B, Schilling TF (1995). Stages of
662 embryonic development of the zebrafish. Development Dynamics. 3, 253-310.
663 https://doi:10.1002/aja.1002030302

Kizil, C., Kaslin, J., Kroehne, V., & Brand, M. (2012). Adult neurogenesis and brain regeneration in zebrafish. *Developmental Neurobiology*, *72*(3), 429–461. https://doi.org/10.1002/dneu.20918

Kroehne, V., Freudenreich, D., Hans, S., Kaslin, J., & Brand, M. (2011). Regeneration of the adult zebrafish brain from neurogenic radial glia-type progenitors. *Development*, *138*(22), 4831–4841. https://doi.org/10.1242/dev.072587

Kuil, L. E., Chauhan, R. K., Cheng, W. W., Hofstra, R. M. W., & Alves, M. M. (2021). Zebrafish: A Model Organism for Studying Enteric Nervous System Development and Disease. *Frontiers in Cell and Developmental Biology*, *8*. https://doi.org/10.3389/fcell.2020.629073

Kunze, W. A. A., & Furness, J. B. (1999). The enteric nervous system and regulation of intestinal motility. *Annual Review of Physiology*, *61*, 117–142. https://doi.org/10.1146/annurev.physiol.61.1.117

Laranjeira, C., Sandgren, K., Kessaris, N., Richardson, W., Potocnik, A., Vanden Berghe, P., & Pachnis, V. (2011). Glial cells in the mouse enteric nervous system can undergo neurogenesis in response to injury. *Journal of Clinical Investigation*, *121*(9), 3412–3424. https://doi.org/10.1172/JCI58200

Lee, E., Song, C. H., Bae, S. J., Ha, K. T., & Karki, R. (2023). Regulated cell death pathways and their roles in homeostasis, infection, inflammation, and tumorigenesis. *Experimental and Molecular Medicine*, *55*(8), 1632–1643. https://doi.org/10.1038/s12276-023-01069-y

Luck, M. S., Dahl, J. L., Boyeson, M. G., & Bass, P. (1993). Neuroplasticity in the smooth muscle of the myenterically and extrinsically denervated rat jejunum. *Cell and Tissue Research*, *271*(2), 363–374. https://doi.org/10.1007/BF00318623

März, M., Chapouton, P., Diotel, N., Vaillant, C., Birgit Hesl, M. T., Lam, C. S., Kah, O., Bally-Cuif, L., & Strähle, U. (2010). Heterogeneity in Progenitor Cell Subtypes in the Ventricular Zone of the Zebrafish Adult Telencephalon. *GLIA*, 58 (7), 370–88. doi: 10.1002/glia.20971

Niesler, B., Kuerten, S., Demir, I. E., & Schäfer, K. H. (2021). Disorders of the enteric nervous system — a holistic view. *Nature Reviews Gastroenterology and Hepatology*, *18*, 393–410. https://doi.org/10.1038/s41575-020-00385-2

Ohno, M., Nikaido, M., Horiuchi, N., Kawakami, K., & Hatta, K. (2021). The enteric nervous system in zebrafish larvae can regenerate via migration into the ablated area and proliferation of neural crest-derived cells. *Development*, *148*(2). https://doi.org/10.1242/dev.195339

Olden, T., Akhtar, T., Beckman, S. A., & Wallace, K. N. (2008). Differentiation of the Zebrafish Enteric Nervous System and Intestinal Smooth Muscle. *Genesis*, *46*(9), 484–498. doi: 10.1002/dvg.20429

Reimer, M. M., Sörensen, I., Kuscha, V., Frank, R. E., Liu, C., Becker, C. G., & Becker, T. (2008). Motor neuron regeneration in adult zebrafish. *Journal of Neuroscience*, *28*(34), 8510–8516. https://doi.org/10.1523/JNEUROSCI.1189-08.2008

Roach, G., Heath Wallace, R., Cameron, A., Emrah Ozel, R., Hongay, C. F., Baral, R., Andreescu, S., & Wallace, K. N. (2013). Loss of ascl1a prevents secretory cell differentiation within the zebrafish intestinal epithelium resulting in a loss of distal intestinal motility. *Developmental Biology*, *376*(2), 171–186. https://doi.org/10.1016/j.ydbio.2013.01.013

710 Romero, M. M. G., McCathie, G., Jankun, P., & Roehl, H. H. (2018). Damage-induced
711 reactive oxygen species enable zebrafish tail regeneration by repositioning of
712 Hedgehog expressing cells. *Nature Communications*, *9*(1), 4010.
713 https://doi.org/10.1038/s41467-018-06460-2
714 Roy-Carson, S., Natukunda, K., Chou, H. chao, Pal, N., Farris, C., Schneider, S. Q., &
715 Kuhlman, J. A. (2017). Defining the transcriptomic landscape of the developing
716 enteric nervous system and its cellular environment. *BMC Genomics*, *18*(1), 1–24.
717 https://doi.org/10.1186/s12864-017-3653-2
718 Rueckert, H., & Ganz, J. (2022). How to Heal the Gut's Brain: Regeneration of the
719 Enteric Nervous System. *International Journal of Molecular Sciences*, *23*(9).
720 https://doi.org/10.3390/ijms23094799
721 Sharrock, A. V., Mulligan, T. S., Hall, K. R., Williams, E. M., White, D. T., Zhang, L.,
722 Emmerich, K., Matthews, F., Nimmagadda, S., Washington, S., Le, K. D., Meir-
723 Levi, D., Cox, O. L., Saxena, M. T., Calof, A. L., Lopez-Burks, M. E., Lander, A. D.,
724 Ding, D., Ji, H., … Mumm, J. S. (2022). NTR 2.0: a rationally engineered prodrug-
725 converting enzyme with substantially enhanced efficacy for targeted cell ablation.
726 *Nature Methods*, *19*, 205–215. https://doi.org/10.1038/s41592-021-01364-4
727 Curado, S., Anderson, R. M., Jungblut, B., Mumm, J., Schroeter, E., & Stainier, D. Y.
728 (2007). Conditional targeted cell ablation in zebrafish: a new tool for regeneration
729 studies. *Developmental dynamics*. 236(4), 1025-1035.
730 https://doi.org/10.1002/dvdy.21100
731 Soret, R., Schneider, S., Bernas, G., Christophers, B., Souchkova, O., Charrier, B.,
732 Righini-Grunder, F., Aspirot, A., Landry, M., Kembel, S. W., Faure, C., Heuckeroth,
733 R. O., & Pilon, N. (2020). Glial Cell-Derived Neurotrophic Factor Induces Enteric
734 Neurogenesis and Improves Colon Structure and Function in Mouse Models of
735 Hirschsprung Disease. *Gastroenterology*, *159*(5), 1824-1838.e17.
736 https://doi.org/10.1053/j.gastro.2020.07.018
737 Stavely, R., Rahman, A. A., Mueller, J. L., Leavitt, A. R., Han, C. Y., Pan, W., Kaiser, K.
738 N., Ott, L. C., Ohkura, T., Guyer, R. A., Burns, A. J., Koppes, A. N., Hotta, R., &
739 Goldstein, A. M. (2024). Mature enteric neurons have the capacity to reinnervate
740 the intestine with glial cells as their guide. *Neuron*, *112*(18), 3143-3160.e6.
741 https://doi.org/10.1016/j.neuron.2024.06.018
742 Taylor, C. R., Montagne, W. A., Eisen, J. S., & Ganz, J. (2016). Molecular fingerprinting
743 delineates progenitor populations in the developing zebrafish enteric nervous
744 system. *Developmental Dynamics*, *245*(11), 1081–1096.
745 https://doi.org/10.1002/dvdy.24438
746 Tokui, K., Sakanaka, M., & Kimura, S. (1994). Progressive reorganization of the
747 myenteric plexus during one year following reanastomosis of the ileum of the
748 guinea pig. *Cell & Tissue Research*, *277*, 259–272.
749 https://doi.org/10.1007/BF00327773
750 Uyttebroek, L., Shepherd, I. T., Harrisson, F., Hubens, G., Blust, R., Timmermans, J.-P.,
751 & Nassauw, L. Van. (2010). Neurochemical Coding of Enteric Neurons in Adult and
752 Embryonic Zebrafish (Danio rerio). *J Comp Neuro*, *518*(21), 4419–4438.
753 https://doi.org/10.1002/cne.22464

754 Wallace, K. N., Akhter, S., Smith, E. M., Lorent, K., & Pack, M. (2005). Intestinal growth
755 and differentiation in zebrafish. *Mechanisms of Development*, *122*(2), 157–173.
756 https://doi.org/10.1016/j.mod.2004.10.009
757 Webb, J. F., Shirey, J. E., Desvignes, T., Carey, A., Postlethwait, J. H., Kimmel, S. R., &
758 Ullmann, B. (2009). *Staging by externally visible anatomy of the living fish*. 238(12),
759 2975-3015. doi: 10.1002/dvdy.22113
760 Westerfield, M. (2000). *A Guide for the Laboratory Use of Zebrafish Danio*
761 *(Brachydanio) rerio* (4th, Ed.). Institute of Neuroscience, University of Oregon,
762 Eugene. Published by the University of Oregon Press.
763 White, D. T., Sengupta, S., Saxena, M. T., Xu, Q., Hanes, J., Ding, D., Ji, H., & Mumm,
764 J. S. (2017). Immunomodulation-accelerated neuronal regeneration following
765 selective rod photoreceptor cell ablation in the zebrafish retina. *Proceedings of the*
766 *National Academy of Sciences of the United States of America*, *114*(18), E3719–
767 E3728. https://doi.org/10.1073/pnas.1617721114
768 Xie, X., Mathias, J. R., Smith, M. A., Walker, S. L., Teng, Y., Distel, M., Köster, R. W.,
769 Sirotkin, H. I., Saxena, M. T., & Mumm, J. S. (2012). Silencer-delimited
770 transgenesis: NRSE/RE1 sequences promote neural-specific transgene expression
771 in a NRSF/REST-dependent manner. *BMC Biology*, *10*(1), 93.
772 https://doi.org/10.1186/1741-7007-10-93
773 Zhang, Y., Ouyang, J., Qie, J., Zhang, G., Liu, L., & Yang, P. (2019). Optimization of the
774 Gal4/UAS transgenic tools in zebrafish. *Applied Microbiology and Biotechnology*,
775 *103*(4), 1789–1799. https://doi.org/10.1007/s00253-018-09591-0
776
777
778
779
780
781
782
783
784
785
786
787
788
789
790
791
792
793

794
795
796
797
798 **Supplementary figures**
799

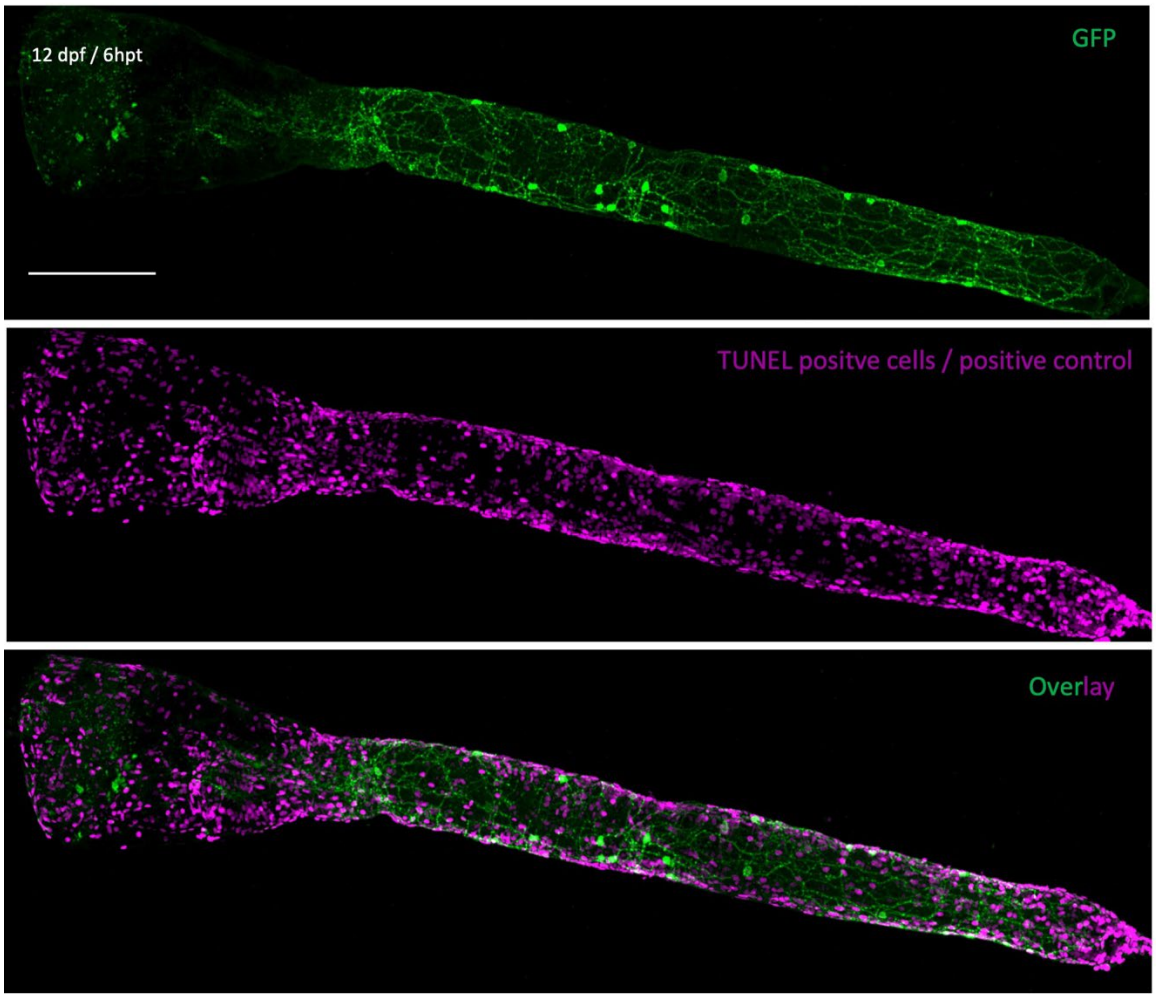

Figure S1: Inducing cell death shows an expected increase in TUNEL+ cells. Inducing cell death as a positive control results in a high number of TUNEL-positive cells (magenta, middle panel) in YFP+ control (green) larvae at 6 hpt (n= 9 larvae, 2 experiments). Maximum projection confocal images of dissected intestine. Scale bar = 100 µm; hpt = hours post treatment.

800

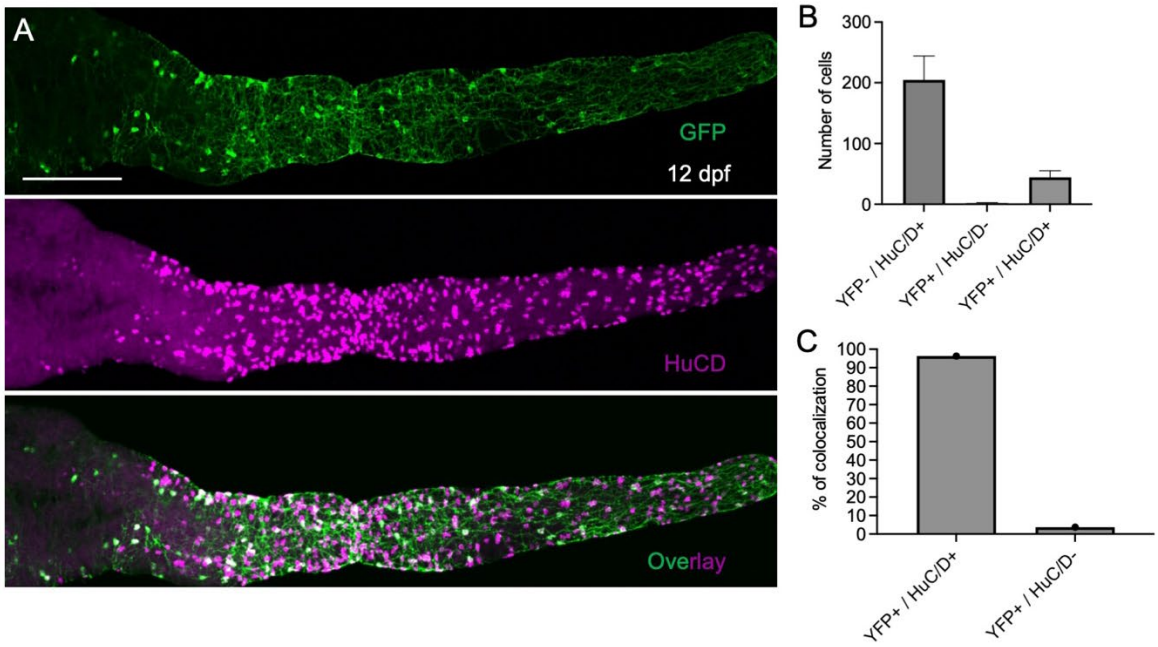

Figure S2. The majority of the YFP+ cells are ENS neurons at 12 dpf

(A) At 12 dpf, YFP+ cells {(labeled with anti-GFP (top, green)} and the pan-neuronal marker HuC/D+ cells (middle, magenta) show high amount of colocalization (bottom, overlay; n= 10 larvae, 2 experiments). **(B)** Bar graph shows the quantification of GFP+/HuC/D+, GFP+/HuC/D- and GFP-/HuC/D+ cells. **(C)** Bar graph shows the percentage of YFP+ cells that are HuC/D+ and HuC/D- cells. Data presented as mean ± SD; Scale bar = 100 μm. dpf = days post fertilization.

801

802

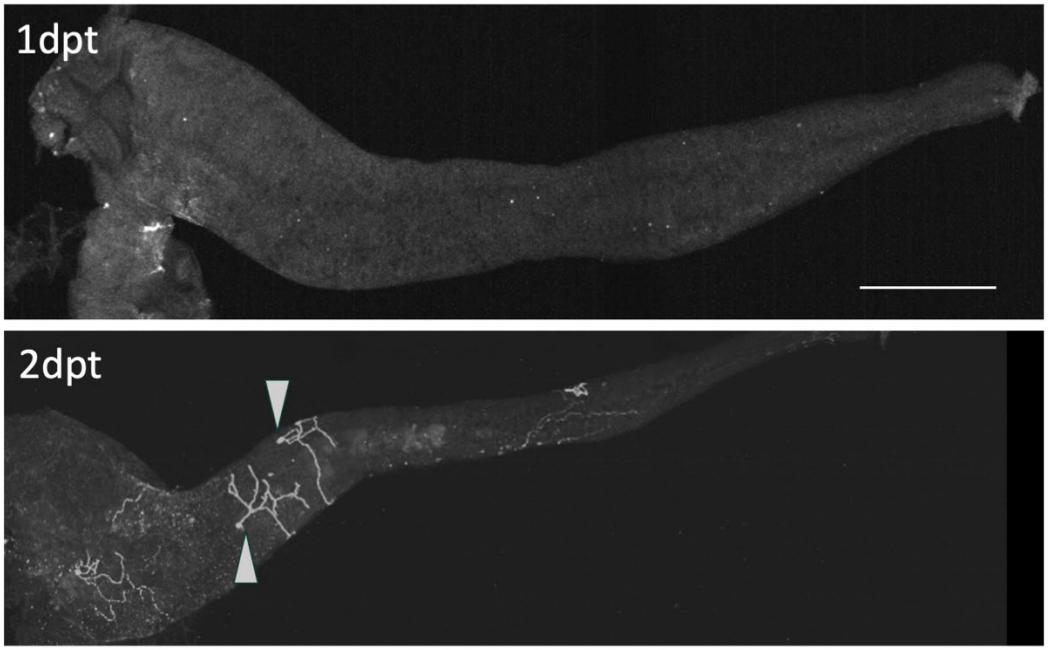

Figure S3. Regenerating neurites in YFP+ neurons following ablation.
At 2 dpt, newly generated YFP+ neurons form neurites as the beginning step of neuron regeneration. Upper panel: at 1 dpt there is complete ablation of YFP+ neurons. Lower panel: at 2 dpt developing neurites that form a bridge (arrow) between the newly generated neurons (6 larvae, 2 experiments). Maximum projection of confocal image of dissected intestine. Scale bar = 100 μm; dpt = days post treatment

803
804
805
806
807

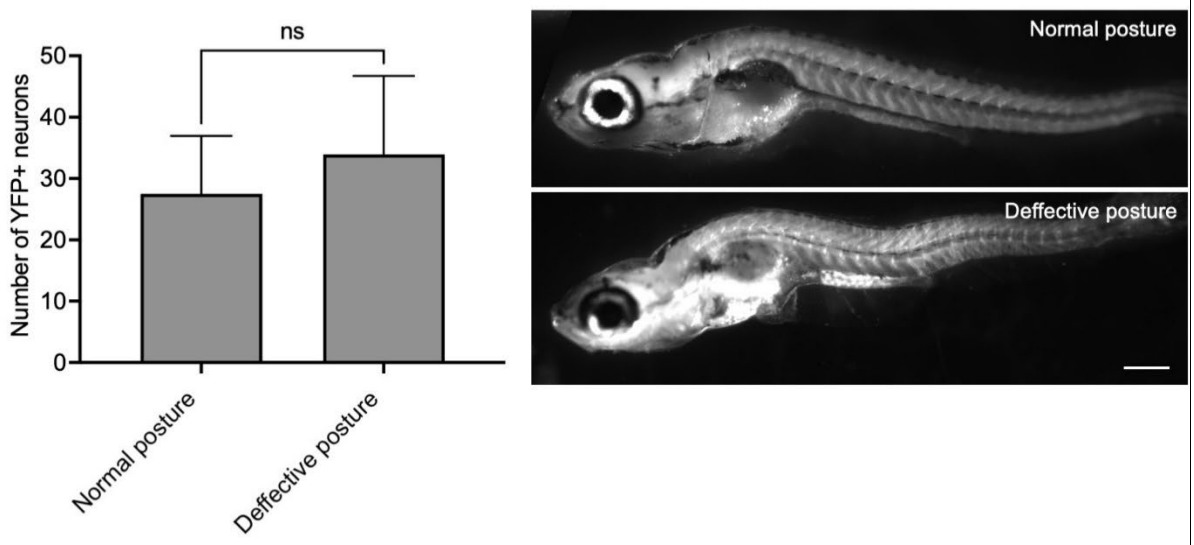

Figure S4. Abnormalities in body posture does not affect YFP+ neurons regeneration. Left panel: The bar graph shows the number of regenerated YFP+ neurons in normally developed larvae compared to those with defective body posture at 12 days post treatment (n = 8 larvae, 2 experiments). Right panel: Whole-mount side views of larvae at stage indicated. Data presented as mean ± SD; ns = no statistically significant differences. Scale bar = 100 µm.

808

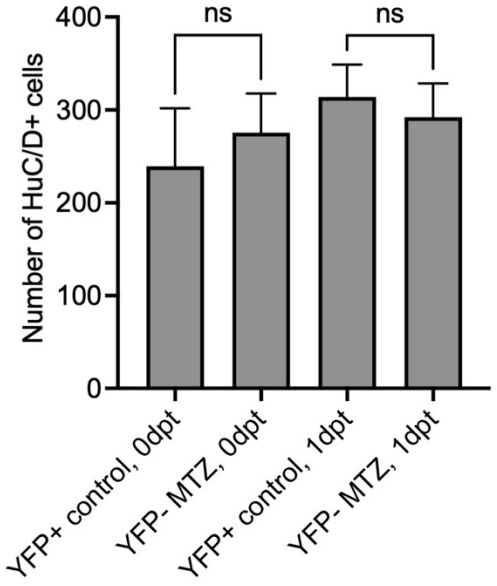

Figure S5. MTZ treatment of YFP- larvae does not affect neuron numbers.

Quantification of HuC/D+ neurons in the gut in YFP- MTZ treated and YFP+ untreated controls at 12dpf (before MTZ treatment) and 13dpf (after MTZ treatment). Bar graph shows the number of HuC/D+ cells. No significant difference was observed between treatment groups (n = 10 larvae, 2 experiments). Data presented as mean ± SD; ns = not significant, dpt = days post treatment.

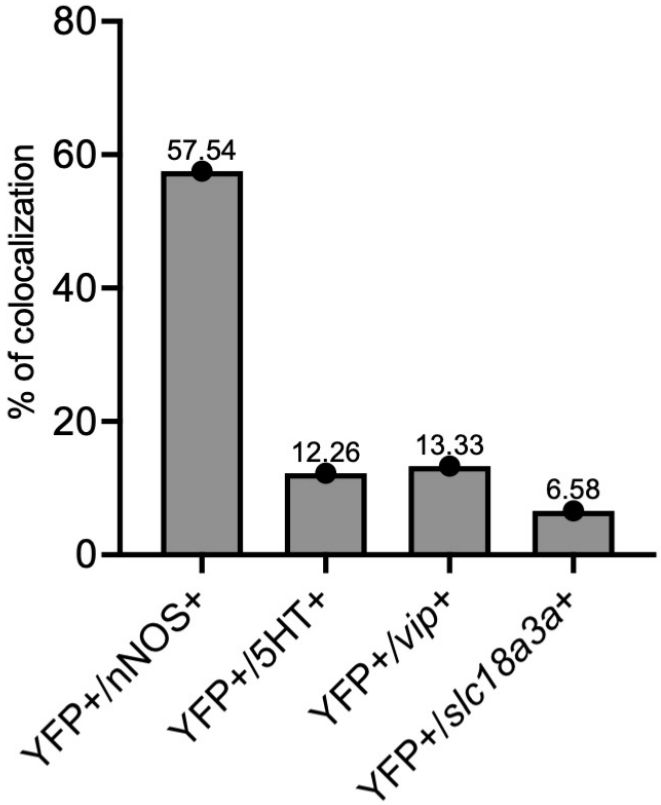

Figure S6. The YFP+ neuronal population consists of different neuronal subtypes at 12 days post fertilization. Quantification of YFP and neuronal subtype colocalization. Bar graph shows the percentage of co-expression of each subtype marker with YFP at 12 days post fertilization / 0 day post treatment (n = 10 larvae, 2 experiments). Data presented as mean.

Supplementary videos have been uploaded to the designated repository.

Groups	Video description
1dpt	Video S1 = YFP- MTZ Video S2 = YFP+ control

	Video S3 = YFP+ MTZ
3dpt	Video S4 = YFP- MTZ Video S5 = YFP+ control Video S6 = YFP+ MTZ
9dpt	Video S7 = YFP- MTZ Video S8 = YFP+ control Video S9 = YFP+ MTZ
dpt = days post treatment	

813